Recycling of Golgi-resident Glycosyltransferases through the ER Reveals a Novel Pathway and Provides an Explanation for Nocodazole-induced Golgi Scattering

Brian Storrie,* Jamie White,‡ Sabine Röttger,‡ Ernst H.K. Stelzer,‡ Tatsuo Suganuma,§ and Tommy Nilsson‡

*Department of Biochemistry, Virginia Polytechnic Institute and State University, Blacksburg, Virginia 24061-0308; ‡Cell Biology and Biophysics Programme, European Molecular Biology Laboratory, D-69012 Heidelberg, Germany; and §Department of Anatomy, Miyazaki Medical College, Miyazaki, 889-1692 Japan

Abstract. During microtubule depolymerization, the central, juxtanuclear Golgi apparatus scatters to multiple peripheral sites. We have tested here whether such scattering is due to a fragmentation process and subsequent outward tracking of Golgi units or if peripheral Golgi elements reform through a novel recycling pathway. To mark the Golgi in HeLa cells, we stably expressed the Golgi stack enzyme *N*-acetylgalactosaminyltransferase-2 (GalNAc-T2) fused to the green fluorescent protein (GFP) or to an 11–amino acid epitope, VSV-G (VSV), and the *trans*/TGN enzyme β1,4-galactosyltransferase (GalT) fused to GFP. After nocodazole addition, time-lapse microscopy of GalNAc-T2–GFP and GalT–GFP revealed that scattered Golgi elements appeared abruptly and that no Golgi fragments tracked outward from the compact, juxtanuclear Golgi complex. Once formed, the scattered structures were relatively stable in fluorescence intensity for tens of minutes. During the entire process of dispersal, immunogold labeling for GalNAc-T2–VSV and GalT showed that these were continuously concentrated over stacked Golgi cisternae and tubulovesicular Golgi structures similar to untreated cells, suggesting that polarized Golgi stacks reform rapidly at scattered sites. In fluorescence recovery after photobleaching over a narrow (FRAP) or wide area (FRAP-W) experiments, peripheral Golgi stacks continuously exchanged resident proteins with each other through what appeared to be an ER intermediate. That Golgi enzymes cycle through the ER was confirmed by microinjecting the dominant-negative mutant of Sar1 (Sar1p^{dn}) blocking ER export. Sar1p^{dn} was either microinjected into untreated or nocodazole-treated cells in the presence of protein synthesis inhibitors. In both cases, this caused a gradual accumulation of GalNAc-T2–VSV in the ER. Few to no peripheral Golgi elements were seen in the nocodazole-treated cells microinjected with Sar1p^{dn}. In conclusion, we have shown that Golgi-resident glycosylation enzymes recycle through the ER and that this novel pathway is the likely explanation for the nocodazole-induced Golgi scattering observed in interphase cells.

Key words: Golgi apparatus • endoplasmic reticulum • Sar1p • protein cycling • nocodazole

THE mammalian Golgi apparatus is the central organelle within the secretory pathway. It plays an important role in processing, maturation, and sorting of newly synthesized secretory and membrane proteins received from the ER and in recycling receptors involved in endocytosis (for reviews see Palade, 1975; Rothman, 1994). It also has major roles in general complex carbohydrate and glycolipid biosynthesis and lipid processing. The overall distribution of the Golgi apparatus varies considerably from cell type to cell type and from organism to organism. In plants and fungi, the individual Golgi units are scattered about the cytoplasmic volume in a series of flattened sets of stacked cisternae. In mammalian fibroblasts, on the other hand, individual Golgi units are clustered together in a juxtanuclear array, often termed the Golgi ribbon, in close association with microtubules and the microtubule organizing center. When visualized by immunofluorescence, the Golgi ribbon appears as a lacy structure occupying a volume of 5–7 μm in length, 1–2 μm in breadth, and 3–5 μm in depth (Storrie and Kreis, 1996). When viewed

The first two authors contributed equally to the paper.

Requests for plasmids or cell lines from within North America should be directed to Brian Storrie and from within the European Union to Tommy Nilsson.

Address correspondence to Brian Storrie (after December 31, 1998), Department of Biochemistry, Virginia Polytechnic Institute and State University, Blacksburg, VA 24061-0308. Tel.: (540) 231-6434. Fax: (540) 231-9070. E-mail: storrie@vt.edu

by electron microscopy in single thin sections, the organelle appears as long ribbons of interconnecting tubules and stacks of cisternae highly enriched in specific resident proteins such as glycosyltransferases. In thick sections, the Golgi complex consists of a flattened set of cisternae with tubular and vesicular arrays and the whole interconnected by tubules between cisternal stacks (Rambourg and Clermont, 1990). Golgi cisternae can be distinguished from one another by their relative content of resident glycosylation enzymes. In cell fractionation experiments, Golgi cisternae differ slightly in density from one another; enzymes acting early in the modification of N-linked oligosaccharides are found to be separated, albeit partially, in distribution from those acting later (Dunphy et al., 1981; Dunphy and Rothman, 1983). By electron microscopy, glycosylation enzymes exhibit distinct, but overlapping, gradient-like distribution patterns (Nilsson et al., 1993; Rabouille et al., 1995*a*; Röttger et al., 1998). Whereas β1,4-galactosyltransferase (GalT)[1] is found mainly in the *trans*-cisternae and the TGN, the *O*-glycosylation enzyme *N*-acetylgalactosaminyltransferase-2 (GalNAc-T2) is found throughout the Golgi stack with a somewhat higher preference for the *trans*-cisternae (Röttger et al., 1998). Hence, GalT provides a subcompartment-specific marker for the *trans*/TGN and may be used to assess the polarity of Golgi stacks, whereas GalNAc-T2 provides a general marker for the Golgi stack.

The steady-state distribution of Golgi glycosylation enzymes is thought to be, in part, the result of recycling, either through retrograde transport vesicles, tubular connections between cisternae, direct transport to the ER, or some combination of these possibilities (for review see Nichols and Pelham, 1998). Such recycling is suggested by the addition of agents such as brefeldin A or nocodazole. Brefeldin A results in a rapid redistribution of the Golgi apparatus into the ER (Doms et al., 1989; Lippincott-Schwartz et al., 1989), while nocodazole induces a slow dispersal of the juxtanuclear Golgi to peripheral sites (Cole et al., 1996*a*; Yang and Storrie, 1998). Both effects indicate an underlying recycling pathway through the ER (for review see Storrie and Yang, 1998). A direct test for such a pathway was carried out recently by the Lippincott-Schwartz laboratory and demonstrated recycling to the ER of chimeric proteins that localized to the Golgi (Cole et al., 1998). In these experiments, the temperature-sensitive domain of vesicular stomatitis virus G protein (VSV-G^{ts}) provided a trap for chimeric protein accumulation in the ER at restrictive temperature. Chimeric proteins for Golgi proteins from the *cis* to *trans* sides all accumulated in the ER under these conditions. In contrast, work from the Warren laboratory argues against recycling of Golgi proteins to the ER (Shima et al., 1998). Microinjection of the dominant-negative mutant of Sar1 ($Sar1p^{dn}$), a small GTPase needed for COP II–mediated export out of the ER, in the presence of nocodazole failed to accumulate in the ER the *medial* Golgi-resident protein giantin under conditions where the intermediate compartment marker, ERGIC53, did. The two opposing lines of evidence, for and against recycling of Golgi-resident proteins through the ER, are not easy to reconcile. However, the time course for the $Sar1p^{dn}$ experiments was relatively short, and it remains a distinct possibility that Golgi-resident proteins recycle through the ER at a slow rate. Such a possibility would be consistent with the slow kinetics of Golgi dispersal observed upon nocodazole-induced microtubule depolymerization.

Here, we have taken the hypothesis that Golgi-resident glycosylation enzymes do recycle through the ER and that this explains the slow reformation of Golgi stacks seen at peripheral sites (Cole et al., 1996*a*; Burkhardt et al., 1997; Yang and Storrie, 1998). We have used green fluorescent protein (GFP)- and epitope-tagged Golgi-resident glycosylation enzymes to examine how individual scattered Golgi elements form over the full time span of microtubule depolymerization. We have also investigated over several hours the effect of microinjecting $Sar1p^{dn}$ on the possible ER accumulation of cisternal glycosyltransferases. In testing our hypothesis, we have formulated four different tests: (*a*) Scattered Golgi structures (stacks) during microtubule depolymerization should form in an episodic manner, similarly to that of the recently reported formation of VSV-G^{ts}–GFP–labeled vesicular–tubular structures at ER exit sites (Presley et al., 1997; Scales et al., 1997). The postulated block in Golgi protein cycling is at the level of juxtanuclear collection of Golgi structures and is post-ER exit. (*b*) Scattered Golgi stacks should exchange proteins with one another on a time scale of tens of minutes in a manner suggestive of an ER intermediate in the exchange process. (*c*) Introduction of $Sar1p^{dn}$ should lead to ER accumulation of preexisting Golgi membrane proteins over a matter of hours. (*d*) $Sar1p^{dn}$ should interfere with nocodazole-induced Golgi scattering and lead to the disappearance of scattered Golgi structures as Golgi-resident proteins now accumulate in the ER. Our overall aim was to investigate whether or not Golgi cisternal proteins cycle. We found that Golgi elements appeared at scattered sites in an abrupt manner without any detectable tracking of fluorescent structures from the juxtanuclear Golgi complex to peripheral sites. Photobleaching experiments showed that scattered Golgi elements slowly exchanged resident proteins. Quantitative morphometric scoring of the distribution of the epitope-tagged Golgi marker GalNc-T2–VSV indicated that, at all time points during the scattering process, GalNAc-T2 resided predominantly in stacked cisternae of normal number and length, albeit sometimes curved in morphology. In favorable sections, the Golgi stacks were observed in close association with budding ER regions (ER exit sites). Introduction of $Sar1p^{dn}$ in the presence of protein synthesis inhibitors resulted in the slow disappearance of juxtanuclear GalNAc-T2 and GalT localization with a corresponding ER accumulation. Thus, the predictions of our four tests were met. We conclude from these results that there exist an ongoing recycling of Golgi proteins through ER and that this is a significant pathway in vivo. Moreover, we suggest it is this process that underlies the abrupt formation of Golgi stacks at peripheral sites in nocodazole-treated cells.

1. *Abbreviations used in this paper:* CHX, cycloheximide; FRAP, fluorescence recovery after photobleaching over a narrow area; FRAP-W, fluorescence recover after photobleaching over a wide area; GalNAc-T2, *N*-acetylgalactosaminyltransferase-2; GalT, β1,4-galactosyltransferase; GFP, green fluorescent protein; PDI, protein disulfide isomerase; VSV-G, vesicular stomatitis virus G protein.

Materials and Methods

Preparation of Plasmids Coding for Recombinant GFP Fusion Proteins or Sar1pH79G

GalT–GFP and GalNAc-T2–GFP were constructed by fusing the stalk region of either GalT or GalNAc-T2 to the NH_2 terminus of GFP. DNA fragments encoding the cytoplasmic, transmembrane, and stalk regions were generated by PCR with an EcoRI site and a consensus Kozak sequence at the 5′ end and a BamHI site at the 3′ end. The primers used for GalT were 5′ GAA TTC GAA TTC GCC ATG AGG CTT CGG GAG CCG CT 3′ (forward primer) and 5′ GGA TCC GGA TCC CGG GGC ACT GGG ACC GAG GTC AA 3′ (reverse primer) to amplify a 361-bp fragment from the full-length GalT cDNA (sequence data available from GenBank/EMBL/DDBJ under accession number X55415) corresponding to amino acids 1–120 of the GalT protein. The primers used for GalNAc-T2 were 5′ GAA TCC GAA TCC GCC ATG CGG CGG CGC TCG CGG ATG 3′ (forward primer) and 5′ GGA TCC GGA TCC CGA AGC TTA TCA CTC TCC AC 3′ (reverse primer) to amplify a 338-bp fragment from the full-length GalNAc-T2 cDNA (accession number X85019) corresponding to amino acids 1–114 of the GalNAc-T2 protein. The PCR fragments encoding the cytoplasmic, transmembrane, and stalk regions were digested with EcoRI and BamHI and ligated into EcoRI-BamHI–digested pEGFP-N1 from CLONTECH Laboratories (Palo Alto, CA; accession number U55762) to generate pGalNAc-T2–GFP and pGalT–GFP. Inserts were checked by sequencing both strands twice using flanking primers.

The pET-11 plasmid encoding Sar1pH79G ($Sar1p^{dn}$) was a generous gift from Dr. W.E. Balch (Scripps Research Institute, La Jolla, CA) and encodes an NH_2-terminally His-tagged, GTP-bound mutant of Sar1a from CHO (Aridor et al., 1995). For expression in mammalian cells, the pET-11 encoding $Sar1p^{dn}$ was digested with NdeI immediately before the start codon. A self complementary synthetic oligonucleotide, 5′ TAGCGG-GATCCAGATCTGGATCCCGC 3′, encoding a BamHI site and a Kozak consensus sequence was then inserted. The resulting construct was then sequenced, and the $Sar1p^{dn}$ insert was then excised and inserted into pCMUIV (pSar1p^{dn}CMUIV) (Nilsson et al., 1989) for transient expression in HeLa cells upon microinjection.

Cell Culture, Transfection, and Nocodazole Treatment

Monolayer HeLa cells (No. CCL 185; American Type Culture Collection, Rockville, MD) were routinely cultured in DME supplemented with 10% fetal calf serum, penicillin (100 U/ml), and streptomycin (100 μg/ml). For generation of stable transfectants, plasmids encoding GalNAc-T2–GFP or GalT–GFP were transfected into HeLa cells cultured in 10-cm tissue culture dishes in the presence of 5% fetal calf serum using the calcium phosphate protocol as described (Pääbo et al., 1986). Selection was for ~3 wk in the above medium supplemented with Geneticin (G-418 sulfate, 400 μg/ml). After significant cell death had occurred and cells began to grow robustly in the presence of Geneticin, cells positive for GFP fluorescence were sorted by a fluorescence-activated cell sorter (FACS® [Becton Dickinson, Sparks, MD], fluorescein filter set, excitation with 488 Argon-ion laser line). The GFP-positive cells were recultured to expand the cell population. Cells were re-sorted as needed to maintain the purity of the population.

In most experiments, cells were exposed to nocodazole at a concentration of 10 or 20 μM with no prior cold pretreatment (Yang and Storrie, 1998). Control experiments established that 10 and 20 μM nocodazole gave identical effects. Nocodazole perfusion experiments were performed in a FCS2 chamber (Bioptechs, Butler, PA; http://www.bioptechs.com) mounted on the microscope stage. GalNAc-T2–GFP or GalT–GFP HeLa cells were grown on 40-mm coverslips and pretreated with 100 μg/ml cycloheximide for at least 15 min. A prenocodazole image was then acquired, and nocodazole at 20 μM plus cycloheximide at 100 μg/ml in complete DME medium was gravity-perfused into the chamber. Perfusion time was typically less than 60 s. The image was refocused and the time series started. For fluorescence recovery after photobleaching over narrow (FRAP) or wide area (FRAP-W) experiments, GalNAc-T2–GFP or GalT–GFP HeLa cells grown on 15-mm coverslips were chilled on ice for 10 min and then warmed to 37°C in the presence of 20 μM nocodazole. Cells were incubated at 37°C in a CO_2 incubator for at least 6 h to scatter the Golgi completely. The coverslip cultures were then transferred to complete medium containing 20 μM nocodazole plus 100 μg/ml cycloheximide and mounted at 37°C in a small aluminum slide chamber (Parton et al., 1992).

Microinjection of pSar1p^{dn}CMUIV and Sar1p^{dn}

Purified plasmid was microinjected into cell nuclei using either an Eppendorf microinjection system (Hamburg, Germany) or a Zeiss automated injection system (AIS; Carl Zeiss, Jena, Germany). The plasmid concentration was 140 ng/μl. The coinjection marker was Cascade blue bovine serum albumin (Molecular Probes, Eugene, OR) at a concentration of 3.33 mg/ml. In some cases, the microinjections were done in either the presence of nocodazole (10 μM) to depolymerize microtubules and/or cycloheximide (100 μg/ml) or emetine (5 μg/ml) (Sigma, Deisenhofen, Germany) to inhibit protein synthesis. $Sar1p^{dn}$ was purified essentially as described by Rowe and Balch (1995). The protein at a concentration of 1.5 mg/ml was microinjected directly into the cytoplasm of HeLa cells. The coinjection marker was Cascade blue bovine serum albumin. Injections were carried out in the presence of 5 μg/ml emetine, and the cells were incubated after injection in the continued presence of emetine.

Antibodies

Affinity-purified rabbit polyclonal antibodies directed against the VSV-G epitope (CPYTDIEMNRLGK; Kreis, 1986) have been described previously (Röttger et al., 1998). Rabbit N10 polyclonal antibodies recognizing human GalT polypeptide have also been described previously (Watzele et al., 1991). Affinity-purified rabbit polyclonal antibodies recognizing GFP were a gift from Dr. Ken Sawin (Cell Cycle Laboratory, Imperial Cancer Research Fund, London, UK) and have been described previously (Shima et al., 1997). Mouse monoclonal antibody 1D3 directed against protein disulfide isomerase (PDI) was a gift from Dr. Stephen Fuller (European Molecular Biology Laboratory [EMBL-Heidelberg]). Mouse monoclonal antibody GTL2 directed against GalT was prepared by T. Suganuma. Cy3-conjugated donkey anti–rabbit or –mouse IgG antibodies were obtained from Jackson ImmunoResearch Laboratories (West Grove, PA). Gold-conjugated goat anti–rabbit secondary antibodies were from British BioCell (Cardiff, UK).

Conventional and Live Cell Confocal Fluorescence Microscopy

For conventional fluorescence microscopy, cells cultured on coverslips were fixed either with −20°C methanol (Ho et al., 1989, 1990), or in the case of microinjected cells, with 3% formaldehyde in PBS. Formaldehyde-fixed cells were permeabilized with 0.5% Triton X-100 in PBS. Immunolabeling, observation with either Zeiss IM-35 or Zeiss Axiovert TV100 microscopes, and photography with either a Photometrics (Tucson, AZ) SenSys charge-coupled device (CCD) camera or a Hamamatsu 3-chip color CCD camera (Open Lab, Improvision, Coventry, UK) were as described (Yang and Storrie, 1998). Optimal visualization of GalNAc-T2–VSV distribution in the ER of microinjected cells with the Hamamatsu 3-chip CCD camera (8-bit intensity range per chip) frequently required overexposure of the fluorescence intensity present in juxtanuclear Golgi of noninjected cells.

For live cell microscopy, cells were viewed with either a Zeiss Axiovert TV100 microscope or an EMBL-Heidelberg confocal modified Zeiss Axioplan microscope. Cells were maintained on the microscope stage at 37°C in an FCS2 chamber or in a small aluminum slide chamber in complete DME medium that had been preequilibrated in a CO_2 incubator. The small chamber was heated by conduction through the immersion oil from a heated objective. This maintains the cells under immediate observation at 37°C. Conventional fluorescence images were acquired with a Hamamatsu high-speed CCD camera at 50-ms time resolution (Open Lab; Improvision, Coventry, UK). All confocal images were acquired on the Compact Confocal Camera (CCC) built at EMBL-Heidelberg, using a 488-nm argon-ion laser line for GFP excitation, a NT80/20/543 beamsplitter and a 505 longpass emission filter, with a 63× 1.4 NA Planapochromat III DIC objective (Carl Zeiss). Typically, a single, unaveraged confocal slice (pinhole 40–50 μm) was taken at each time point with a 20–40-μs integration time per pixel. One image frame was typically collected every 10 or 20 s. Over a series of experiments, illumination was varied so that the images were either unsaturated or brighter structures were saturated in order to visualize dimmer structures. To increase the depth of field, the pinhole was opened completely. In FRAP/FRAP-W experiments, a prebleach image was acquired, and then a rectangular area was bleached with

high-power (953.39 μW) laser light for 20–100 scans at ~1 s per scan. Recovery sequences were imaged identically to the nocodazole perfusion experiments. FRAP/FRAP-W experiments were repeated several times with different sized bleach areas.

Image Processing, Analysis of Fluorescence Intensity, and Calculation of Apparent Rate Constant

All fluorescence image processing was done with Power Macintosh computers using the public domain software NIH Image v1.62b18 (developed at the U.S. National Institutes of Health and available on the Internet at http://rsb.info.nih.gov/nih-image) and the Open Lab System 2.0 (Improvision). Animations of time series were analyzed either with or without 2 or 3 frame running averaging. Images were often displayed using log-up or γ-corrected lookup tables to emphasize dim structures. Analysis of average fluorescence intensity per structure in time-lapse microscopy of nocodazole-treated GalNAc-T2–GFP cells were as previously described (Presley et al., 1997). In brief, full time-lapse image sets were displayed, and structures were tracked from individual time frame to frame at 2× screen "blow-up" with the magnification tool and circled, and the measure function of the analyze menu was used for fluorescence quantification. The measure function calculates an average intensity per pixel within the circled area. Fluorescence recovery in small area photobleaching experiments was quantified by averaging the fluorescence per structure over the entire population of five to six structures included within the inscribed rectangle. An apparent rate constant for recovery based on diffusion theory was calculated using the radius of the circle enclosed within the square bleach area and equations developed by Axelrod et al. (1976). Micrographs were arranged for figures with Adobe Photoshop 4.0.1 (San Jose, CA).

Immunoelectron Microscopy

HeLa cells were fixed for 3 h in 2% paraformaldehyde and 0.2% glutaraldehyde in 0.2 M sodium phosphate buffer, pH 7.4, and embedded in 10% gelatin in PBS. Sample preparation, ultrathin sectioning, and immunolabeling were performed as described previously (Nilsson et al., 1993). For single-labeling, sections of HeLa cells expressing GalNAc-T2–VSV or GalNAc-T2–GFP were incubated with affinity-purified polyclonal antibodies detecting the tag sequence. For double-labelings with two polyclonal antibodies, sections were fixed after the first labeling in 2% paraformaldehyde and 0.2% glutaraldehyde for 10 min and the labeling procedure was repeated with a rabbit polyclonal antibody recognizing endogenous GalT. For double-labelings with one monoclonal and one polyclonal antibody, sections were incubated simultaneously with both primary antibodies, followed by two separate incubations with the appropriate gold-conjugated secondary antibodies. Antibody dilutions were 1:100 to 1:200 for anti–VSV, 1:50 for anti-GalT (N10), 1:10 for anti-PDI, and 1:100 for all gold-conjugated goat anti–rabbit secondary antibodies (British BioCell). After immunolabeling, sections were positively stained and embedded with 2% methyl cellulose containing 0.3% uranyl acetate (Tokuyasu, 1978), air-dried, and viewed in a Zeiss EM10 at 80 kV.

Quantification of Electron Micrographs

The labeling densities of expressed GalNAc-T2 (10 nm gold) over Golgi stacks, nonstacked Golgi associated membrane profiles, ER, and mitochondria were determined by the point-hit method (Weibel, 1979). GalNAc-T2–VSV–positive areas were photographed at random, at 34,000 magnification, and negatives scanned using a flat-bed scanner (model Scanmaker III; Mikrotek Lab, Inc., Santa Clara, CA) and printed at a final magnification of 74,000. 15 images were analyzed per each test condition. Golgi stacks were defined as membrane structures containing three or more cisternae that overlap within half or more of their median cisternal length. Nonstacked Golgi-associated membrane profiles (Golgi tubules) were defined as tubular–vesicular structures adjacent to Golgi stacks. A square-lattice grid with a spacing d = 17 mm was used to count the points P corresponding to the grid line intersections with the membranes of the respective structure. Labeling densities were calculated by dividing the number of 10-nm gold particles (GalNAc-T2–VSV) that fall into the boundaries of each type of structure by the product of the number of points of intersection of the structure P with the grid multiplied by d^2. Background labeling was calculated by counting the number of gold particles detected over mitochondria. It was usually less than 2 gold particles/μm^2. Standard errors of the mean were calculated.

To evaluate Golgi stack length for linear and curved Golgi onions, lengths were traced on printed micrographs and converted to micrometers. The length of Golgi ribbons were traced with the map tool; a Golgi ribbon is defined as a continuous GalNAc-T2–VSV labeling pattern with no gaps of more than 0.2 μm. The number of cisternae per Golgi stack, be it linear or curved into an onion structure, were counted by direct inspection of prints. Mean lengths and cisternal numbers were counted for each time of nocodazole treatment, and the standard error of the mean was calculated. Control histograms of length distributions and cisternal number indicate that the mean values are a fair comparative parameter. Micrograph sets were assembled into figures using Adobe Photoshop 4.0.1 software.

Results

Localization of GalNAc-T2–GFP and –VSV in Untreated and Nocodazole-treated Cells

To address how peripheral Golgi elements form upon microtubule depolymerization, we visualized the scattering process directly in living cells and morphometrically characterized the ultrastructural products of Golgi scattering. As Golgi markers, we chose GalNAc-T2 and GalT. Both glycosyltransferases are type II transmembrane proteins and localize to the Golgi apparatus with high specificity. Endogenous GalNAc-T2 is found across the entire Golgi stack, with a distribution skewed slightly towards the *medial*- and *trans*-cisternae (Röttger et al., 1998). Endogenous GalT has a more polarized distribution towards the *trans*-Golgi and TGN (Roth and Berger, 1982; Röttger et al., 1998). To label the Golgi in living cells, we expressed chimeric proteins between GalNAc-T2 or GalT and GFP. The respective glycosyltransferase stalk region, sufficient for Golgi localization (for review see Füllekrug and Nilsson, 1998), was fused to the NH_2 terminus of GFP, thus substituting GFP for the lumenal, catalytic domain of the enzyme. We then generated stable HeLa cell lines expressing either GalNAc-T2–GFP or GalT–GFP. Similar GFP fusion proteins have been shown by others to localize properly to the Golgi apparatus (Sciaky et al., 1997; Shima et al., 1997). We show here (confocal microscopy, Fig. 1 *A*) that GalNAc-T2–GFP distributed in live cells in a compact juxtanuclear pattern very similar to that of endogenous or epitope-tagged GalNAc-T2 (Röttger et al., 1998). At the ultrastructural level, immunogold labeling of thawed cryosections showed GalNAc-T2–GFP associated with Golgi stacks (Fig. 1 *B*, *arrowhead*) and tubulovesicular elements adjacent to Golgi stacks (Fig. 1 *B*, *asterisk*). Similarly, we observed a Golgi-specific localization for GalT–GFP consistent with its endogenous distribution (results not shown). GalNAc-T2–GFP and GalT–GFP are thus bona fide markers for the Golgi and Golgi-derived structures in living cells.

To morphometrically characterize Golgi scattering at the ultrastructural level, we immunolabeled GalNAc-T2 tagged with the VSV-G epitope (GalNAc-T2–VSV) in thawed cryosections. Because the GalNAc-T2–VSV/antibody pairing gives abundant and highly Golgi-specific labeling in non-drug treated cells (Röttger et al., 1998), we were able to identify GalNAc-T2–VSV–positive structures regardless of their morphology. Stably expressed GalNAc-T2–VSV has the same quantitative distribution as endogenous GalNAc-T2 but is much easier to detect since it is more abundant and reacts well with affinity-purified poly-

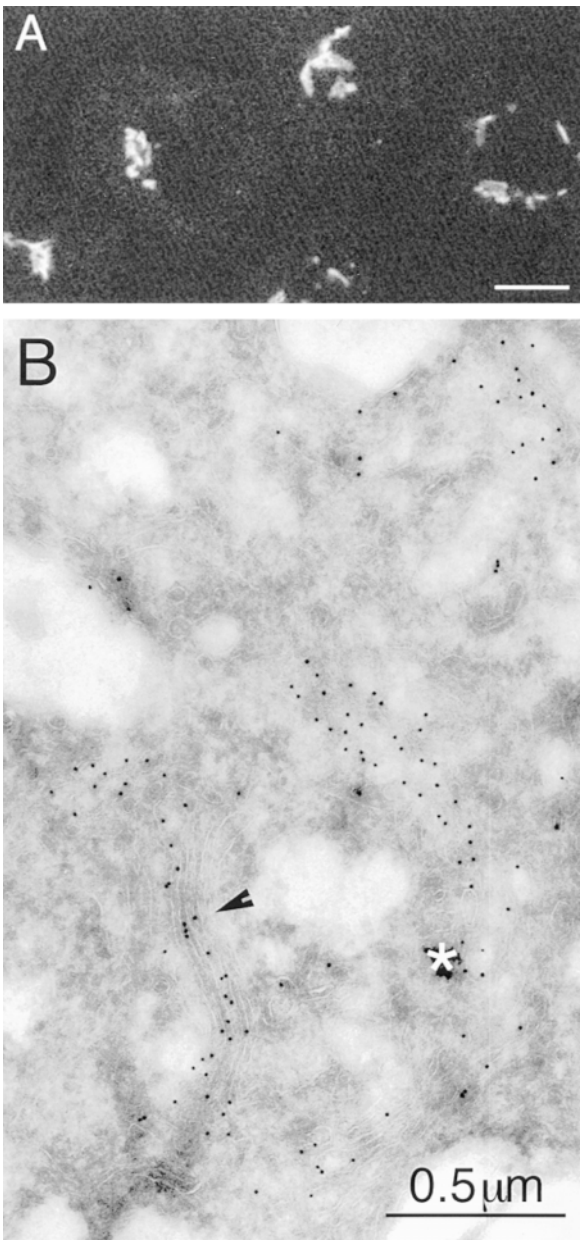

Figure 1. GalNAc-T2–GFP accurately marks the Golgi in vivo. GalNAc-T2–GFP was stably expressed in HeLa cells as described in Materials and Methods. (*A*) GalNAc-T2–GFP in live HeLa cells, confocal microscope image. The fluorescence patterns in the five cells shown are juxtanuclear and in some cases encircle the nucleus. The cells shown have a typical Golgi distribution. (*B*) GalNAc-T2–GFP associates with Golgi stacks and tubulovesicular elements in cryo-EM sections. GalNAc-T2–GFP is revealed by immunogold labeling (10-nm particle size) with a primary antibody directed against GFP. The gold particles are associated with stacked and tubulovesicular elements of a long Golgi ribbon. The black arrowhead points to an example where the section passes perpendicular to a Golgi stack. The asterisk indicates a tubulovesicular region within the Golgi ribbon. Bar in *A*, 20 μm.

clonal anti–VSV-G (Röttger et al., 1998). The time course of nocodazole-induced Golgi scattering in HeLa cells expressing GalNAc-T2–VSV was established by immunofluorescence with the same anti–VSV-G antibody used for our ultrastructural analysis. In agreement with previous studies (Yang and Storrie, 1998), Golgi scattering in HeLa cells was a gradual process, not quite complete at 4 h; full dispersal to peripheral structures was apparent after a 6-h or longer incubation with nocodazole (Fig. 2). Projections of confocal serial sections showed that the fluorescent Golgi markers scattered over the entire volume of the cell excluding the nucleus (data not shown). Nocodazole-induced Golgi scattering did not depend on new protein synthesis. Treatment of cells with cycloheximide at 100 μg/ml before and during nocodazole treatment had no effect on the scattering process for any of the markers (data not shown; Turner and Tartakoff, 1989; Cole et al., 1996*a*; Yang and Storrie, 1998). Thus, existing Golgi-resident transmembrane proteins, including our markers, must somehow migrate or redistribute to generate the peripheral structures.

Peripheral Golgi Structures Appear in an Episodic Manner

We monitored the initial stages of Golgi scattering in live HeLa cells stably expressing GalNAc-T2–GFP or GalT–GFP. Cells were perfused with 20 μM nocodazole in the presence of cycloheximide directly on the confocal microscope stage and then observed over time. Experiments were repeated multiple times, varying nocodazole exposure time, illumination intensity, optics (confocal versus conventional optics), and in some cases pretreating the cells with nocodazole on ice. Similar results were seen un-

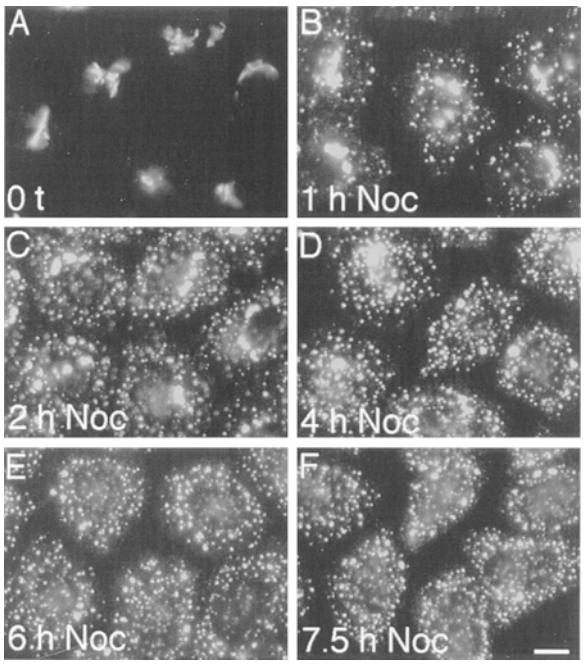

Figure 2. Long-term scattering kinetics of GalNAc-T2 in response to nocodazole-induced microtubule depolymerization. HeLa cells stably transfected with GalNAc-T2–VSV were incubated with nocodazole for the times indicated in the figure. Coverslip cultures were fixed with methanol and then processed for immunofluorescence using affinity-purified rabbit anti–VSV antibodies and Cy3-conjugated anti–rabbit secondary antibodies. Bar, 10 μm.

der all conditions, including conventional rather than confocal optics, where the depth of imaging field was much greater. Golgi scattering was followed for 1–2 h after nocodazole addition. This is the key time period of initial appearance of many individual peripheral Golgi elements. Because of technical limitations in maintaining focal plane, we were unable to follow in living cells the complete kinetics of Golgi scattering over its full 4–6 h time course.

Fig. 3 shows a representative experiment with cells expressing GalNAc-T2–GFP. Single unaveraged confocal scans were collected every 10 s for 1 h after addition of nocodazole. Early after nocodazole addition, the Golgi was a compact structure localized next to the nucleus, occasionally with a few separate elements immediately adjacent (Fig. 3 *A*). Readily apparent peripheral elements first appeared after ~5–10 min and increased in number over the 1-h time span of the experiment (Fig. 3, compare *A* with *K*), although concentrated juxtanuclear fluorescence remained. Animation of the time series showed that individual peripheral elements appeared faintly yet abruptly at a remote site, increased in fluorescent intensity at that site, and then remained stable in both intensity and position. Very rarely did peripheral Golgi elements move over distances of more than 1 μm, and directed movement could not be discerned. To show such movement information in a single image, we averaged images over ~8-min time spans from four different periods, hence sampling the entire time course. Fig. 3 shows three images for each of four

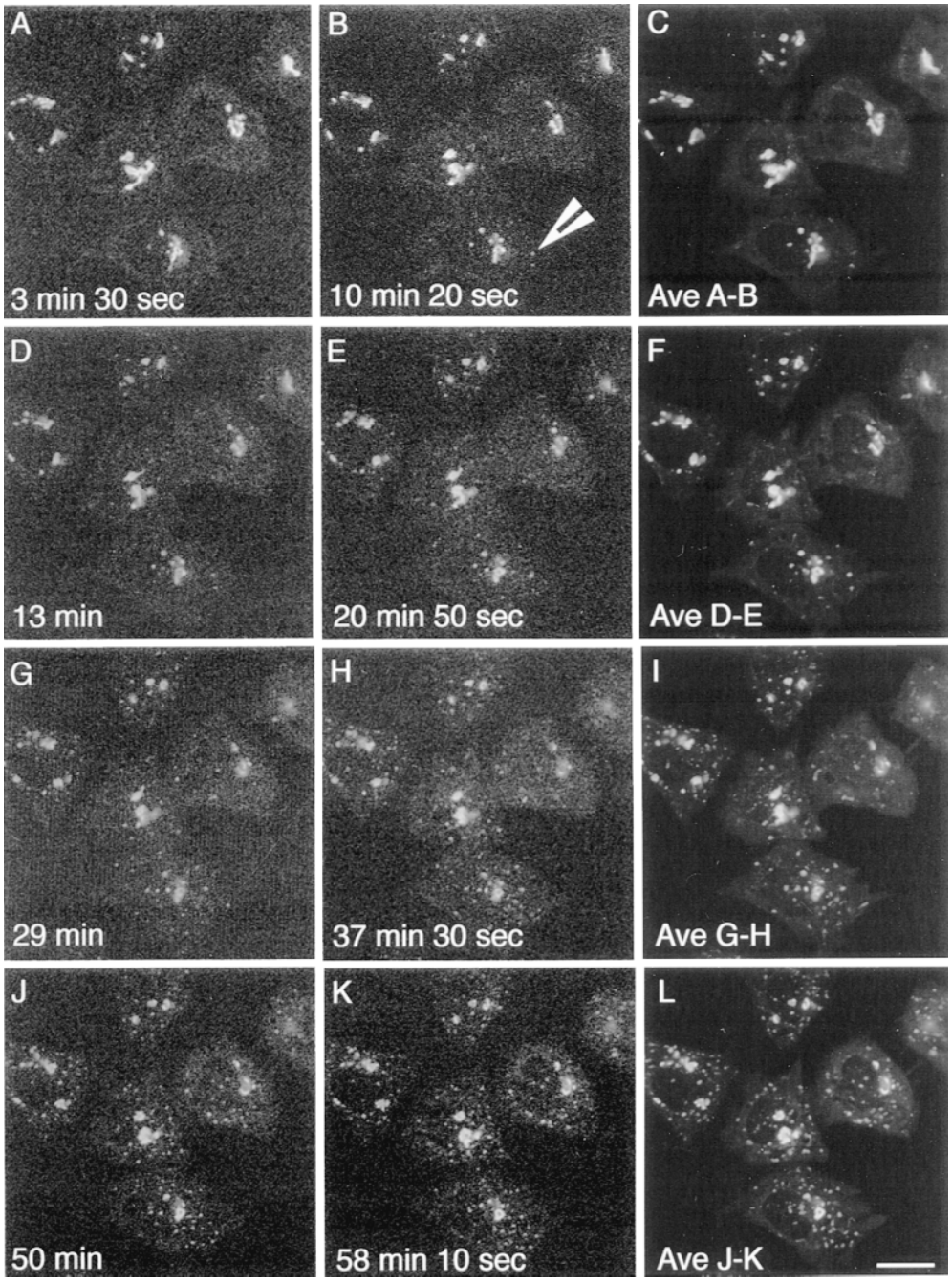

Figure 3. With nocodazole addition, GalNAc-T2–GFP appears at scattered sites with no net outward movement in live cells. HeLa cells stably expressing GalNAc-T2–GFP were incubated with 20 μM nocodazole for the times indicated. Six cells are shown. Unaveraged confocal scans were taken every 10 s for 1 h after nocodazole addition. Four different periods spanning the time course are shown (*A–C*, *D–F*, *G–I*, and *J–L*). The images in the first column (*A*, *D*, *G*, and *J*) are the first time point in the period, the images in the second column (*B*, *E*, *H*, and *K*) are the last time point in the period, and the images in the third column (*C*, *F*, *I*, and *L*) are an average of all time points from the first through the last in the period, inclusive. Peripheral fluorescent patches appear faintly, accumulate fluorescence, and then remain stable in intensity and position. The net number of peripheral patches in a cell increases gradually with time. The averaged frames (*C*, *F*, *I*, and *L*) reveal no net directional movement of fluorescent patches. Bar, 20 μm.

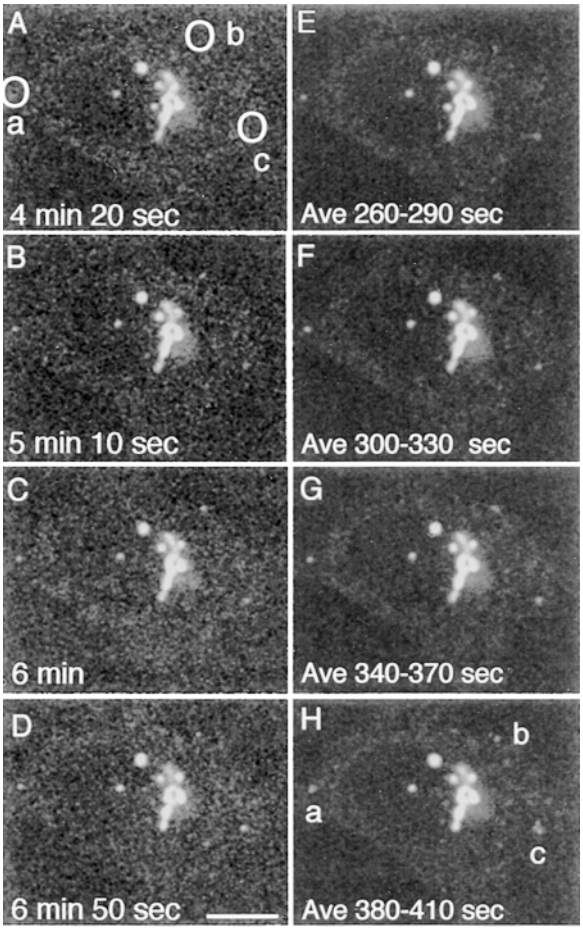

Figure 4. Formation of individual peripheral patches induced by nocodazole treatment. A brief, early time interval was selected from the time-lapse experiment shown in Fig. 3. The abrupt appearance of three peripheral fluorescent patches (marked as *a–c*, in *H*) is shown over a 2.5-min period. *A–D* are individual confocal frames at the indicated time points after nocodazole addition. *E–H* are frame averages over the indicated time intervals in seconds. The circled areas in *A* (*a–c*) will be sites of subsequent fluorescent patch formation. Individual patches appear abruptly (compare *A* and *B*). At first they appear faint (*B*), but they then accumulate fluorescence (compare *B–D*). The averaged frames indicate no net outward directional movement of individual patches from the cell center, although they do oscillate within a small area defined by the smeared regions in the averaged panels (*F–H*). Bar, 10 μm.

periods. The first time point in the period is in the left column (*A*, *D*, *G*, and *J*), the last time point is in the middle column (*B*, *E*, *H*, and *K*), and the average of all images included within each time period is in the right column. In such averaged images, movement of an element over time would produce an elongated smear or a track to nearly continuous trail of fluorescent structures depending on rate of movement, because the element is in a different position in each frame being averaged. We see little such smearing or elongation in the averaged images. Rather, the area that a peripheral Golgi element occupied within a given period showed as a slightly enlarged region of fluorescence relative to a single time frame, indicating that the element moved within a small domain. We examined more closely the appearance of individual elements in a single cell. In Fig. 4, the three elements *a*, *b*, and *c* in *H* first appeared faintly (*B*) at sites near the cell periphery, and then became gradually brighter (compare *B–D*). Four-frame averages covering the time points in *A–D* showed that the three elements do not change position from frame to frame. Similar results were seen with GalT–GFP, although GalT–GFP scattered somewhat more rapidly (data not shown).

To quantify the kinetics of formation of individual peripheral Golgi elements and their stability once formed, we scored the fluorescent intensity of 15 individual peripheral fluorescent elements over time. All 15 individual elements increased linearly in fluorescence intensity for about 2 min, the abrupt formation period, and then were fairly stable in fluorescence over an extended period of time (data not shown). The fluorescence intensity of individual structures was ~3.5–5-fold greater than background. In a further effort to detect intermediates or outward tracking of individual Golgi elements from the juxtanuclear region, similar nocodazole scattering periods were examined at near video rates (20 frames per second) with a high-speed CCD camera and conventional optics. Again appearance at peripheral sites was abrupt and episodic; no outward movements from the juxtanuclear region were observed, and no vesicular intermediates were detected. Thus, time-lapse observation, be it with confocal or conventional optics of GalNAc-T2–GFP and GalT–GFP in live cells, shows that during microtubule depolymerization, peripheral Golgi elements arise abruptly, apparently de novo. Once they appear, peripheral Golgi fragments do not move directionally and increase in fluorescence intensity briefly, accumulating GalNAc-T2–GFP or GalT–GFP, and then become relatively stable. These results are completely consistent with the proposed hypothesis that peripheral Golgi fragments arise due to slow, constitutive cycling of Golgi components followed by abrupt coalescence of these components at or about ER exit sites (Cole et al., 1996*a*; Yang and Storrie, 1998).

Scattered Golgi Structures Consist of Stacked Cisternae

To characterize the structure of nocodazole-scattered, Golgi-derived elements and possible intermediates in their formation, over the full time course of nocodazole-induced Golgi scattering, we fixed HeLa cells stably expressing GalNAc-T2–VSV at 0, 1, 2, 4, and 7.5 h after nocodazole addition and processed them for immunoelectron microscopy with the same anti-VSV antibody used for immunofluorescence experiments. Thawed cryosections were double-labeled with 10-nm gold for the VSV epitope and 5-nm gold for endogenous PDI, an ER marker. We photographed 15 GalNAc-T2–VSV–positive fields at random and scored them morphometrically. Initially (0 time), GalNAc-T2–VSV immunogold labeling was restricted almost exclusively to long, juxtanuclear Golgi ribbons consisting of a mix of stacks and interconnecting tubulovesicular structures (Fig. 5 *A*, 10-nm gold). The essentially continuous ribbons of GalNAc-T2–VSV labeling were frequently interrupted by gaps in the labeling continuity such as that shown in Fig. 5 *A* (*white arrow*). Only rarely did PDI label

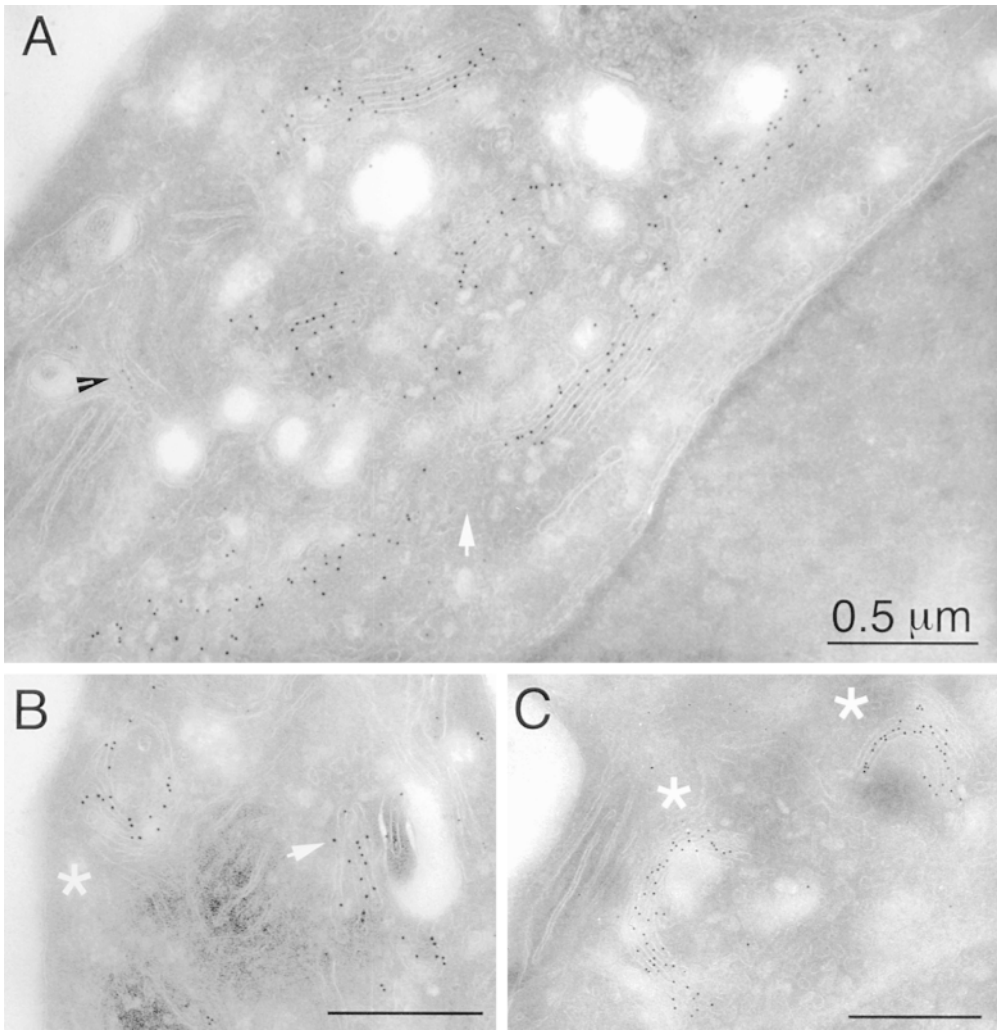

Figure 5. Immunogold localization of GalNAc-T2–VSV shows that the Golgi maintains its stack structure upon nocodazole treatment. HeLa cells stably transfected with GalNAc-T2–VSV were either fixed immediately (*A*) or incubated in the presence of nocodazole for 2 h (*B*) or 7.5 h (*C*). Cryosections were double labeled for GalNAc-T2–VSV (Golgi, 10-nm gold) and PDI (ER, 5-nm gold). As can be seen in *A*, GalNAc-T2–VSV enriched structures in control cells consist of a mix of stacked Golgi cisternae and tubulovesicular structures. Continuous segments of stacked cisternae and tubulovesicular structures are termed a Golgi ribbon. The white arrow points to an example of an interruption that divides an otherwise continuous Golgi ribbon into two segments. The black arrowhead points to PDI in an ER element. In nocodazole-treated cells (*B* and *C*), GalNAc-T2–VSV–enriched structures consist either of linear stacks of Golgi cisternae (*B*, *white arrowhead*) and associated tubulovesicular structures or stacks and associated tubulovesicular structures that curve back on themselves to form onions (*asterisks*, *B* and *C*).

(5-nm gold, Fig. 5 *A*, *black arrowhead*) intermix with GalNAc-T2–VSV. A small amount of PDI was found in the *cis*-Golgi network and in the *cis*-cisternae. After 2 h of nocodazole treatment, GalNAc-T2–VSV was occasionally found in stacked structures that curved back on themselves, which we refer to as onions (Fig. 5 *B*, *asterisk*); more frequently, GalNAc-T2–VSV associated with flattened stacks and tubulovesicular structures (Fig. 5 *B*, *arrow*). After longer nocodazole treatment (4 and 7.5 h), the onion structures became more common (Fig. 5 *C*, *asterisks*). At 7.5 h, onions accounted for ~40% of the stacked Golgi profiles. The onion structures were polarized as indicated by labeling for endogenous GalT, a well-characterized *trans*-Golgi/TGN marker (Roth and Berger, 1982; Röttger et al., 1998), as were the flattened scattered Golgi stacks (Fig. 6). In favorable sections, GalNAc-T2–VSV–positive, scattered Golgi stacks in nocodazole-treated cells appeared to be associated with ER exit sites (data not shown).

Quantitatively, the length of Golgi ribbons, defined as continuous gold-labeled structures with no gaps in labeling, dropped upon nocodazole treatment (Fig. 7 *A*), consistent with previous studies (for review see Burkhardt, 1998). However, over the entire 7.5-h nocodazole exposure, the average length of individual stack units and the number of cisternae per stack stayed rather constant (Fig. 7 *A*). There was a transient decrease in GalNAc-T2–VSV labeling density (gold particles per μm^2) over Golgi-like stacks and tubules (Fig. 7 *B*). At all time points, the density of GalNAc-T2–VSV labeling over the ER was low, ~50–60-fold less than that over Golgi stacks or tubules, and increased only slightly during Golgi scattering (Fig. 7 *B*). In conclusion, our ultrastructural observations show that the bulk of GalNAc-T2–VSV is present in individual Golgi-like structures, cisternal stacks (flattened and onion-like), and associated tubules during the entire period of nocodazole treatment. Since our time-lapse observations of GalNAc-T2– and GalT–GFP in live cells showed that intact stack fragments do not track outward, we suggest that individual Golgi stacks must form de novo at peripheral sites. Additionally, the frequency of Golgi onions increased only after a time lag following nocodazole addi-

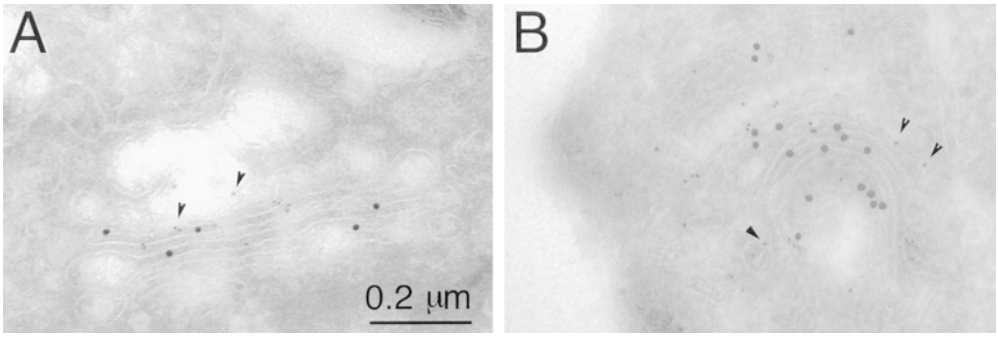

Figure 6. Peripheral Golgi structures are polarized. Both linear (*A*) and onion-shaped Golgi stacks (*B*) in nocodazole-treated cells show a polarized distribution of GalT. HeLa cells stably expressing GalNAc-T2–VSV were incubated with nocodazole for 7.5 h. Cells were then fixed and processed for cryosectioning and immunolabeling with 15-nm gold (GalNAc-T2–VSV) and endogenous GalT (5-nm gold). The black arrowheads point to examples of GalT (5-nm gold) labeling to one side of the Golgi stack. In sections cut perpendicular to Golgi stacks, GalNAc-T2–VSV distributes across much of the stack while GalT is found predominantly to one side.

tion, suggesting that these structures are newly formed, rather than being rearrangements of preexisting Golgi stacks. As we never observed major concentrations of GalNAc-T2–VSV in intermediate structures, individual peripheral Golgi stacks must form and concentrate GalNAc-T2–VSV quickly, in agreement with our observation in live cells that peripheral structures appeared abruptly and then accumulated Golgi-resident proteins rapidly over a very brief time window. These observations are consistent with the proposed hypothesis that cycling Golgi proteins may coalesce at or about ER exit sites to regenerate Golgi stacks de novo.

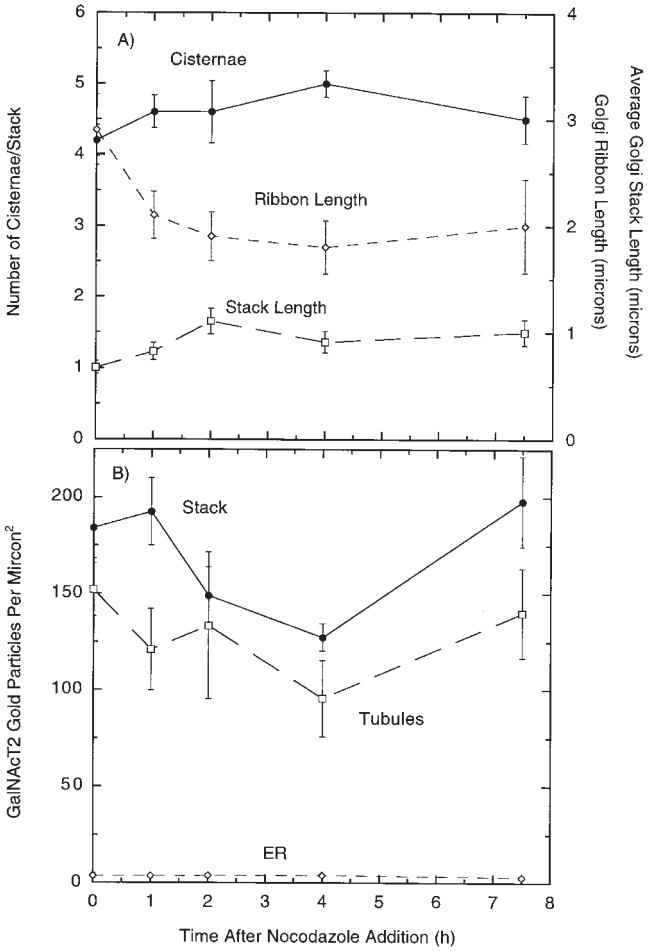

Figure 7. Stacks are maintained, and GalNAc-T2–VSV labeling remains concentrated in cisternae as the Golgi scatters. 15 different images were quantified for each time point. The number of cisternae per stack includes both flattened and curved stacks (*A*). Golgi ribbon length decreases slightly (see Figs. 1 and 5 for visual examples of Golgi ribbons), and stack length actually increases (*A*). GalNAc-T2–VSV labeling distribution over Golgi-like structures dropped transiently during Golgi scattering (*B*). Only a small increase in GalNAc-T2 labeling density over the ER was observed consistent with Golgi proteins concentrating during episodic assembly events into Golgi stacks. Error bars are the standard error of the mean.

Peripheral Golgi Stacks Slowly Exchange Resident Proteins

If Golgi proteins are indeed recycling, then peripheral Golgi stacks may be continuously exchanging resident proteins with each other. As a first step in characterizing whether or not such exchange does occur, we took a photobleaching approach using cells expressing GalNAc-T2–GFP or GalT–GFP. To produce peripheral Golgi stacks, cells were pretreated with nocodazole. We then photobleached GFP fluorescence associated with a subset of these structures. In all experiments, we preincubated cells with 100 μg/ml of cycloheximide for at least 15 min before the bleach and continuously after the bleach, so any recovery must be due to transfer from nonbleached Golgi elements. We repeated the experiments several times, varying the size of the bleached area. When only a small area of the cell was bleached, 5% or less, recovery of fluorescence over the bleached area should be accompanied by no detectable loss of fluorescence over the remainder of the cell. This approach is termed FRAP for fluorescence recovery after photobleaching. From the rate of recovery, an apparent rate constant can be calculated. This is equivalent to an apparent diffusion coefficient. When a large area of the cell was bleached, ~50%, recovery of fluorescence over the bleached area could only occur with significant loss of fluorescence from the remainder of the cell. This approach is termed FRAP-W for fluorescence recov-

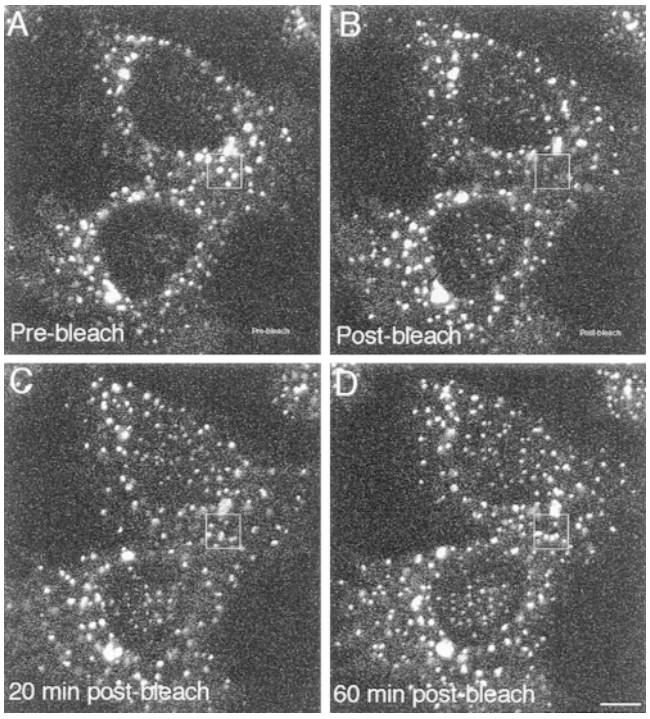

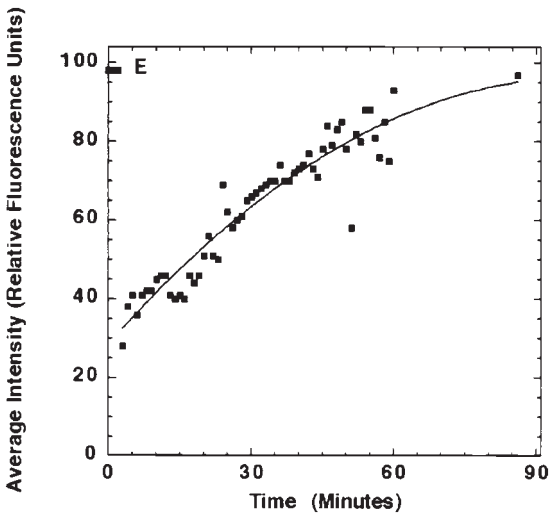

Figure 8. FRAP experiments reveal that resident Golgi proteins are exchanged slowly between peripheral Golgi stacks. Two cells are shown in the center of the field and a portion of a third in the upper right hand corner. Cells were treated with nocodazole for 6 h to scatter the Golgi. The boxed 4 × 4 μm area in the upper center cell was photobleached (*B*). The cells were observed at 10-s intervals for 90 min after the bleach. As shown in *C* and *D*, photorecovery of the peripheral bleached patches was gradual with recovery at the same rate across the entire boxed area. Fluorescence recovery is quantified in *E* as described in Materials and Methods. Zero time is immediately after the bleach (*B*). Bar, 5.0 μm.

ery after photobleaching over wide area. If all peripheral Golgi stacks are active in protein exchange, then at the end of a FRAP-W experiment a reduced level of fluorescence should be observed across the entire organelle population.

Photobleaching of a small area, 4 × 4 μm square, was followed by progressive fluorescence recovery, which was complete within about 90 min and had a half-time of about 35 min (Fig. 8). Interestingly, recovery occurred at the same rate across the entire bleached area, regardless of the distance from the bleach boundary (compare Fig. 8, *C* and *D*). This suggests that the peripheral Golgi stacks were effectively interconnected by a fast exchange network. One such example could be the ER. The apparent rate constant for fluorescence recovery in this representative experiment was 5×10^{-12} cm^2/s, about 1/2,000th the diffusion constant reported for Golgi membrane proteins in intracellular membranes (Storrie et al., 1994; Cole et al., 1996*b*; Ellenberg et al., 1997). As expected for FRAP experiment, there was no detectable loss of fluorescence from the nonbleached areas.

Fig. 9 shows a representative FRAP-W experiment where the bleached area, 32 × 19 μm, was about half of the cell area (Fig. 9, *A* and *B*, *boxed areas*). Fluorescence

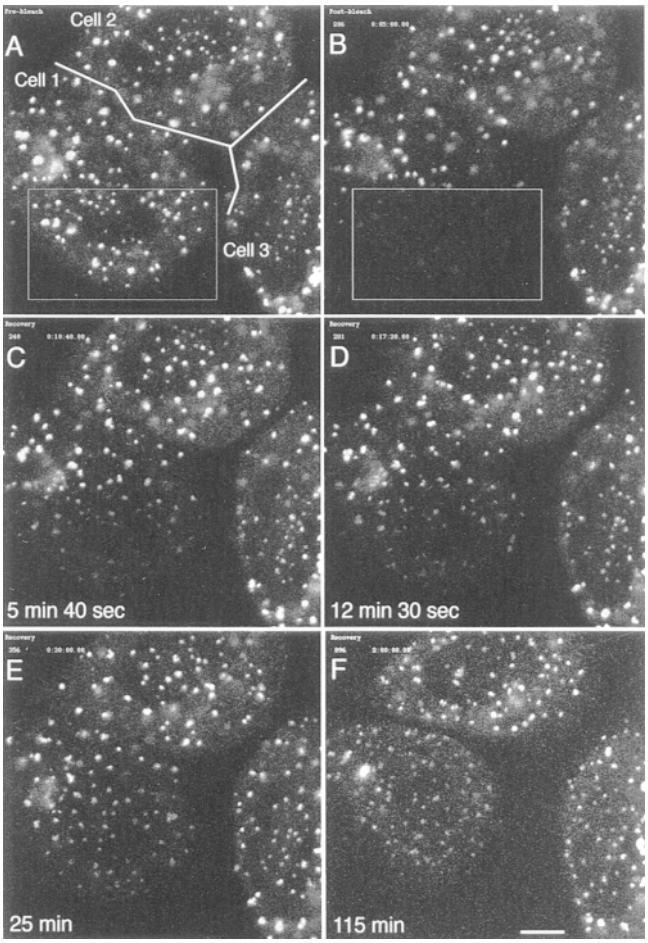

Figure 9. FRAP-W experiments reveal that the entire population of peripheral Golgi stacks are active in protein exchange. Three cells are shown. Cells were treated with nocodazole for 6 h to scatter the Golgi. The boxed area covering cell 1 (*A*, ~50% of cell area) was photobleached (*B*). The cells were observed at 10-s intervals for 2 h after the bleach. As shown in *C–F*, photorecovery of the peripheral bleached patches was gradual. Correspondingly, fluorescence was lost from the nonbleached fluorescent patches. Zero time is immediately after the bleach (*B*). Bar, 7.5 μm.

recovery in the bleached area was gradual, and a loss of fluorescence from the unbleached area accompanied the recovery within the bleached zone. Recovery for this large bleach area was fastest close to the bleach boundary; noticeable recovery was seen within about 5 min in peripheral Golgi elements closest to the bleach boundary (Fig. 9 *C*). At longer times (12–25 min, Fig. 9, *D* and *E*), fluorescence recovery spread further away from the bleach boundary. At the same time, loss of fluorescence from nearby structures in the nonbleached zone became more apparent. Approximately 2 h after bleach, peripheral Golgi elements across cell 1 in Fig. 9 had a fairly uniform, medium-intensity fluorescence, indicating that essentially all peripheral Golgi stacks were active in protein exchange (Fig. 9 *F*). Animation of recovery sequences for either FRAP or FRAP-W experiments suggested that fluorescence reaccumulated into preexisting structures. Little in the way of collisions between adjacent Golgi stacks was apparent. Animation under nonsaturating illumination conditions revealed no obvious exchange intermediates moving into the bleached area. In animations, where illumination was very intense (~100-fold higher than for the recovery sequences), we observed a flickering, lacy fluorescent network interconnecting scattered Golgi elements (data not shown). Within or in close association with this network were often seen mobile concentrations of fluorescent material. These may be intermediates in exchange. This network may be ER containing low levels of GalNAc-T2–GFP or GalT–GFP. Similar results were seen for both GalNAc-T2–GFP and GalT–GFP.

We conclude from these experiments that peripheral Golgi stacks slowly exchange resident transmembrane proteins via a dissociative process. The apparent rate constant for fluorescence recovery was slow relative to known diffusion constants for Golgi membrane proteins in either Golgi or ER membranes (Storrie et al., 1994; Cole et al., 1996*b*; Ellenberg et al., 1997). The flux of fluorescence into the bleached zone during recovery was low, consistent with the low level of GalNAc-T2–VSV seen in ER membranes during nocodazole-induced Golgi scattering.

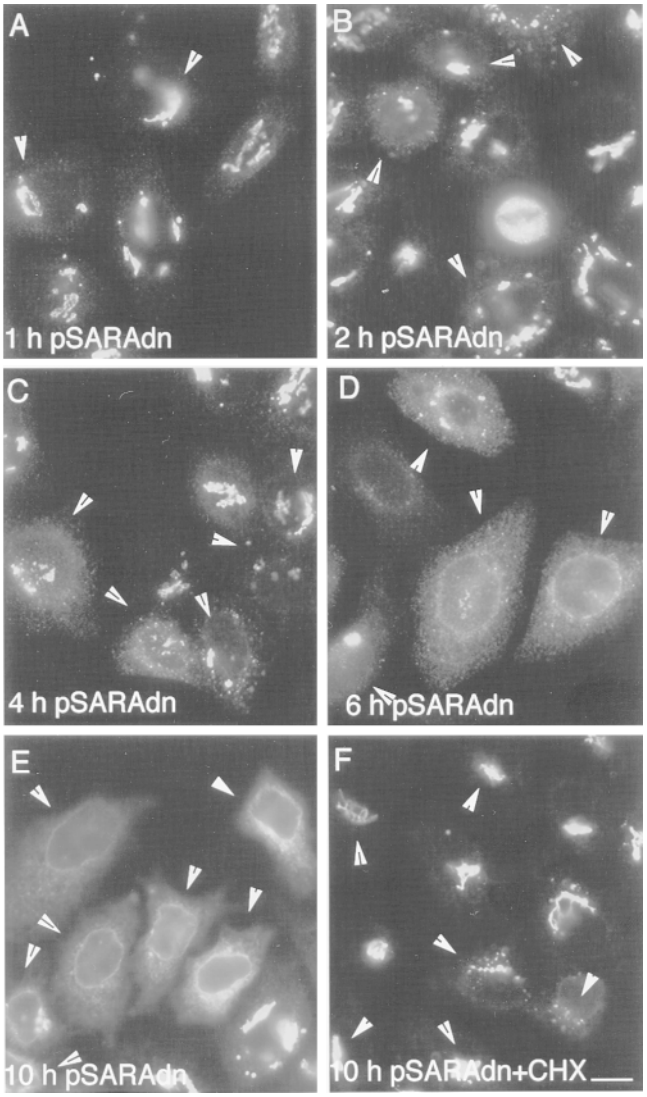

Figure 10. Microinjection of pSar1p^{dn}CMUIV plasmids resulted in the gradual loss of juxtanuclear Golgi staining for GalNAc-T2–VSV and a concomitant accumulation in the ER. Cells were microinjected with plasmid as described in Materials and Methods. Cascade blue bovine serum albumin was used as a coinjection marker. Microinjected cells are indicated by arrowheads. Cells were fixed at various times after injection: *A*, 1 h; *B*, 2 h; *C*, 4 h; *D*, 6 h; *E*, 10 h. After a lag period, as seen in *A*, where there is little if any effect on GalNAc-T2–VSV distribution, progressive accumulation in the ER as marked by a weblike cytoplasmic staining pattern and rim staining of the nucleus was observed. With time, most if not all juxtanuclear concentration of GalNAc-T2 staining was lost. In *F*, cells were microinjected with plasmid in the presence of 100 μg/ml CHX and then incubated for 10 h in the presence of drug. CHX gave almost complete inhibition of GalNAc-T2 redistribution. Bar, 10 μm.

Golgi Glycosyltransferases Slowly Cycle to the ER with Expression of a Dominant-negative Sar1p

The above results suggest that resident Golgi glycosyltransferases, type II transmembrane proteins, normally cycle slowly from the Golgi to the ER and back. In the case of the nocodazole-treated cell, forward transport and juxtanuclear accumulation of these cycling Golgi proteins is blocked because of microtubule depolymerization. To provide direct evidence in support of this putative cycling route, we characterized the effect of a dominant-negative mutant of Sar1p, Sar1p^{dn}, on the distribution of the Golgi glycosyltransferases, GalNAc-T2–VSV and endogenous GalT. Sar1p, a small GTPase, is required for the recruitment of COPII components onto the ER for the formation of export vesicles. Addition of His-tagged Sar1p^{dn} to both in vitro (Aridor et al., 1995) and in vivo assays (Pepperkok et al., 1998; Shima et al., 1998) has been shown to block protein export from the ER. We decided to express Sar1p^{dn} in HeLa cells as a native protein by microinjecting the plasmid pSar1p^{dn}CMUIV encoding the native protein as well as microinjecting a purified His-tagged version of the Sar1p^{dn}. Cycloheximide (CHX) and emetine (Perlman and Penman, 1970) were used as inhibitors of protein synthesis to test that any observed ER accumulations were predominantly of preexisting proteins rather than newly synthesized proteins.

Microinjection of pSar1p^{dn}CMUIV produced after a lag period of 2–3 h, a loss of juxtanuclear Golgi staining for GalNAc-T2–VSV, and appearance of an ER-like staining pattern marked by distinct rim labeling of the nucleus, a characteristic trait of ER labeling, and a diffuse network-like labeling of the cytoplasm (Fig. 10, *arrowheads* point to injected cells). The development of an ER staining pattern for GalNAc-T2–VSV was complete within 6–10 h after microinjection. The disappearance of a juxtanuclear Golgi staining and the development of an ER labeling pattern for GalNAc-T2–VSV was dependent on synthesis of Sar1p^{dn} as indicated by CHX inhibition when the plasmid was injected in the presence of drug and cells subsequently incubated for 10 h in the continued presence of CHX (Fig. 10 *F*). A similar disappearance of juxtanuclear Golgi labeling was seen when cells microinjected with pSar1p^{dn} CMUIV were stained for GalT (data not shown). The kinetics of disappearance appeared similar to that of GalNAc-T2. Because GalT labeling was less bright, the ER accumulation of GalT was more difficult to detect. The image set presented in Fig. 10 was overexposed with respect to the juxtanuclear Golgi staining in non-injected cells in order to emphasize the ER labeling of GalNAc-T2–VSV. The fact that two Golgi glycosyltransferases, one epitope tagged and introduced into HeLa cells by stable transfection and the other endogenous, behaved the same upon Sar1p^{dn} expression suggests that loss of juxtanuclear Golgi staining reflects a general property of the organelle and its membrane proteins.

The pronounced ER accumulation of GalNAc-T2–VSV in Sar1p^{dn}-expressing cells is due to both redistribution of preexisting protein and the accumulation of newly synthesized protein. Three approaches were taken to assess whether or not the predominant accumulation was of preexisting molecules. The first approach was a calculation based on assessment of the metabolic stability of GalNAc-T2–VSV. In control experiments, no loss of GalNAc-T2–VSV antigenicity was observed after 10 h of incubation of HeLa cells in the presence of 100 μg/ml CHX, a concentration sufficient to give 90–95% inhibition of methionine incorporation, or 5 μg/ml emetine, a concentration sufficient to give 99% inhibition of methionine incorporation (data not shown). In these experiments, the same camera exposures were used for non–drug-treated and drug-treated cells, and all pixels were within the linear range of the CCD camera. Hence GalNAc-T2–VSV may be considered to be metabolically stable during the time of our experiments. Considering the 24-h generation time of HeLa cells, >70% of the GalNAc-T2–VSV in cells expressing Sar1p^{dn} for 10 h should be preexisting protein. This percentage is even larger at the 6-h post–plasmid injection time point. Hence the majority of ER accumulation reflected the redistribution of preexisting GalNAc-T2–VSV from a juxtanuclear Golgi to the ER rather than the accumulation of newly synthesized proteins in the ER. As a further test that preexisting molecules had redistributed from a juxtanuclear location, the pSar1p^{dn}CMUIV plasmid was pulse expressed in cells. In this experimental protocol, HeLa cells were microinjected with the plasmid, and then at either 1 h or 3 h after injection, CHX or emetine was added to inhibit further protein synthesis. The cells were then fixed 10 h post-injection and the distribution of

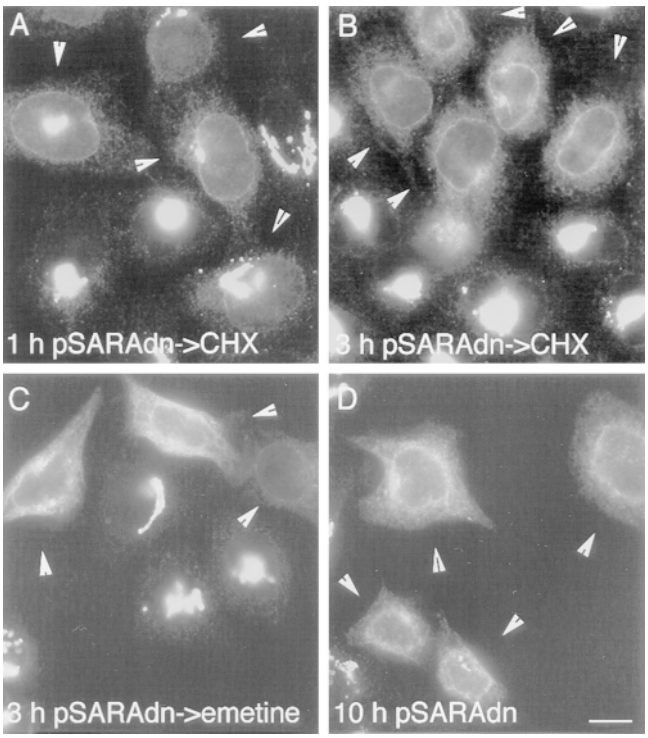

Figure 11. Pulse expression of Sar1p^{dn} was sufficient to give GalNAc-T2–VSV redistribution to the ER. Cells were microinjected as described in Materials and Methods and the legend for Fig. 10. Cells were incubated for various times after injection in the absence of protein synthesis inhibitor. (*A*) CHX at a concentration of 100 μg/ml was added 1 h after plasmid injection. Cells were then incubated in the presence of drug for an additional 9 h. (*B*) CHX was added 3 h after microinjection, and cells were incubated for an additional 7 h. (*C*) Emetine was added at a concentration of 5 μg/ml, and the cells were then incubated for an additional 7 h. (*D*) Cells were incubated in the absence of drug for 10 h after microinjection. Bar, 10 μm.

GalNAc-T2–VSV assessed. As shown in Fig. 11, expression of plasmid into protein for periods as short as 1 h was sufficient to produce ER accumulation of GalNAc-T2–VSV and substantial decrease in juxtanuclear Golgi staining. 3 h of pulse expression limited by either CHX or emetine addition was sufficient to give full control disappearance of juxtanuclear Golgi staining. As a final test, purified His-tagged Sar1p^{dn} was microinjected into cells in the presence of emetine, and the cells were then incubated afterwards in the continuous presence of emetine. Cells were then stained either for GalNAc-T2 or GalT. Immunofluorescence staining for GalNAc-T2–VSV showed the beginnings of a nuclear ER-like rim distribution, 1 h after injection. At later time points, a disappearance of juxtanuclear GalNAc-T2–VSV staining was observed with kinetics similar to those of the plasmid expression with accumulation in the ER (Fig. 12, *A* and *C*). As shown in Fig. 12, *B* and *D*, juxtanuclear endogenous GalT staining decreased greatly under these conditions. At 1 h after injection, there were hints of faint, ER-like GalT rim staining of the nucleus in microinjected cells. We conclude that the ER ac-

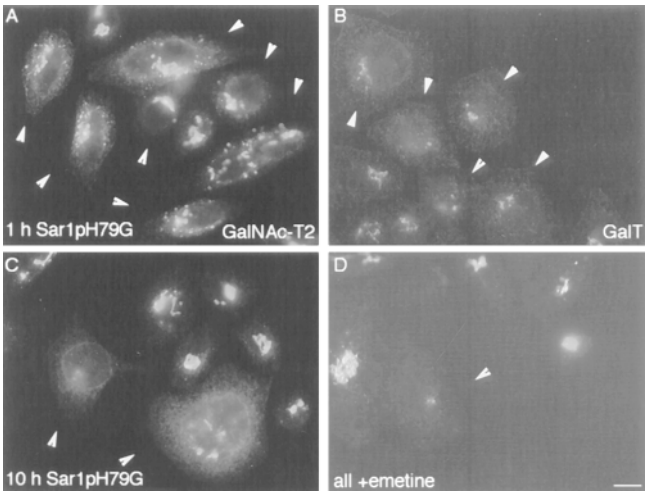

Figure 12. Sar1p^{dn} induced ER accumulation of GalNAc-T2–VSV or GalT by Sar1p^{dn} protein injection. Cells were microinjected with Sar1p^{dn} protein in the presence of 5 μg emetine and then incubated for various times (*A* and *B*, 1 h; *C* and *D*, 10 h) in the presence of emetine. This concentration of emetine is sufficient to inhibit 99% of cellular protein synthesis. Cascade blue bovine serum albumin was used as a coinjection marker. Microinjected cells are indicated by arrowheads. In *A* and *C*, staining is for GalNAc-T2–VSV, and in *B* and *D*, staining is for GalT. Bar, 10 μm.

cumulation was indeed of preexisting Golgi proteins redistributed from the juxtanuclear Golgi.

Expression of Sar1p^{dn} Inhibits Formation of Peripheral Golgi Stacks

To test whether nocodazole-induced Golgi scattering is indeed related to resident Golgi protein cycling to the ER, we performed two additional experiments. In the first, cells pretreated with nocodazole to scatter the Golgi were microinjected with pSar1p^{dn}CMUIV and then assayed for GalNAc-T2–VSV distribution after various plasmid expression periods in the continued presence of nocodazole. In the second, microinjected cells preexpressing Sar1p^{dn} for 3 h were treated with nocodazole to initiate Golgi scattering and assayed for GalNAc-T2–VSV distribution. As shown in Fig. 13 (*arrowheads* point to injected cells), after nocodazole pretreatment (here 5 h) GalNAc-T2–VSV was distributed in scattered fluorescent staining structures. With expression of plasmid after a lag period of about 3 h, there was a progressive disappearance of most to nearly all the peripheral Golgi structures and an ER accumulation of GalNAc-T2. These kinetics were similar, albeit perhaps slightly slower, than that for disappearance of the juxtanuclear Golgi upon plasmid expression. As shown in Fig. 14 (*arrowheads* point to injected cells) with Sar1p^{dn} preexpression, addition of nocodazole for 1 h failed to produce the relatively extensive initial phase of nocodazole-induced Golgi scattering seen in adjacent noninjected cells. In the microinjected cells, ER accumulation of GalNAc-T2 was often apparent as indicated, in particular, by nuclear rim staining. We conclude from these experiments that Golgi transmembrane proteins in nocodazole-treated cells cycle through the ER.

Discussion

The underlying rationale behind these experiments came from our previously stated hypothesis that Golgi transmembrane proteins cycle from the Golgi stack to the ER and back (Storrie and Yang, 1998; Yang and Storrie, 1998). This hypothesis was prompted by our recent observations in both Vero and HeLa cells that during microtubule depolymerization, *trans*-Golgi/TGN type II membrane proteins appeared in peripheral structures more rapidly than comparable *medial*/*trans*-Golgi membrane proteins (Yang and Storrie, 1998) and in HeLa cells that disruption of cytoplasmic dynein function resulted in nocodazole-like Golgi scattering (Burkhardt et al., 1997). From these data, we hypothesized that there might be direct trafficking of Golgi proteins to the ER with subsequent juxtanuclear accumulation being blocked at or about ER exit sites by the nocodazole-induced depolymerization of microtubules (Yang and Storrie, 1998) or inactive motor proteins (Burkhardt et al., 1997). The same hypothesis based on a different set of data from nocodazole experiments has been proposed by Lippincott-Schwartz and colleagues (Cole et al., 1996*a*). In the present work,

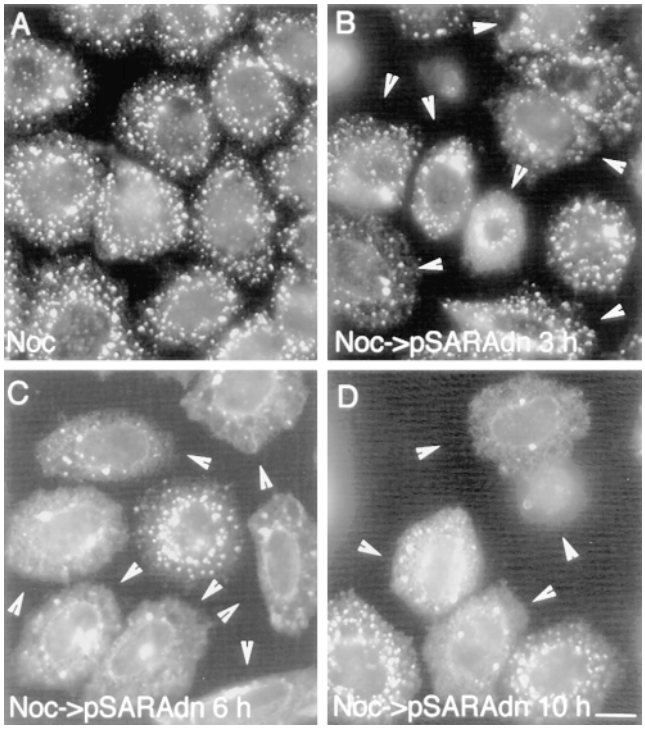

Figure 13. GalNAc-T2–VSV associated with nocodazole peripheral Golgi stacks redistributed to the ER in cells expressing Sar1p^{dn}. Cells were preincubated with nocodazole (*Noc*) for 6 h before microinjection. Plasmid microinjection was as described in Materials and Methods. Cascade blue bovine serum albumin was used as a coinjection marker. Microinjected cells are indicated by arrowheads. Cells were fixed at various times after injection: *B*, 2 h; *C*, 6 h; *D*, 10 h. Nuclear rim staining and diffuse staining of weblike cytoplasmic fluorescence indicate ER localization. Bar, 10 μm.

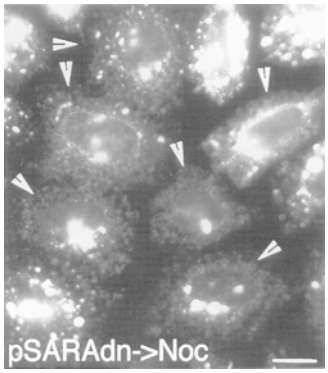

Figure 14. Expression of Sar1p^{dn} inhibited nocodazole-induced Golgi scattering. After microinjection, cells were incubated for 3 h before nocodazole addition. This was to allow for plasmid expression and accumulation of Sar1p^{dn}. Plasmid microinjection was as described in Materials and Methods. Cascade blue bovine serum albumin was used as a coinjection marker. Microinjected cells are indicated by arrowheads. Cells were fixed 1 h after nocodazole addition. Bar, 10 μm.

we have formulated and conducted four different tests of this hypothesis: (*a*) Peripheral Golgi structures (stacks) during microtubule depolymerization should form in an episodic manner similar to that of the recently reported formation of ts-G–GFP–labeled vesicular–tubular structures at ER exit sites (Presley et al., 1997; Scales et al., 1997). The postulated block in Golgi protein cycling is at the level of juxtanuclear collection of Golgi structures and is post-ER exit. (*b*) Peripheral Golgi stacks should exchange proteins with one another on a time scale of tens of minutes in a manner suggestive of an ER intermediate in the exchange process. (*c*) Expression of Sar1p^{dn}, known to block ER exit, should lead to ER accumulation of preexisting Golgi membrane proteins. (*d*) Expression of Sar1p^{dn} should interfere with nocodazole-induced Golgi scattering and lead to the disappearance of scattered Golgi structures as the proteins present in these structures accumulate in the ER. Here, we find that the outcome of each test supports our fundamental hypothesis. In stating these positive conclusions in support of a novel pathway, we would like to acknowledge that the present experiments are only a step towards elucidating the nature of this pathway. Future experiments will determine to what extent this pathway recycles Golgi proteins in relation to other possible recycling pathways.

To test whether or not peripheral Golgi structures (stacks) appeared in an episodic manner during microtubule depolymerization, we expressed two chimeric proteins, GalNAc-T2–GFP and GalT–GFP, to fluorescently mark the Golgi in living HeLa cells and used our previous construct, GalNAc-T2–VSV (Röttger et al., 1998), as an abundant, epitope-tagged analogue for ultrastructural studies. All three chimeras are from well-characterized, type II, Golgi-resident, transmembrane proteins. GalNAc-T2 was chosen for most experiments because it provides a marker for the entire Golgi stack with only limited preference for one part of the stack, *trans* over *cis* (Röttger et al., 1998). Microtubule depolymerization was induced by addition of the drug nocodazole. By correlating GalNAc-T2–GFP fluorescence distribution in living cells and GalNAc-T2–VSV immunogold labeling in thawed cryosections, we were able to assess the trafficking and organizational state of the Golgi complex continuously during its scattering in response to microtubule depolymerization. We found that individual stacked Golgi elements formed at peripheral cytoplasmic sites in a burst-like or episodic manner. We never observed preexisting Golgi elements tracking outward from the juxtanuclear Golgi complex to peripheral sites. Rather, individual Golgi elements appeared abruptly at peripheral cytoplasmic sites with no detectable intermediates. Once formed, these structures were stable for tens of minutes, maintaining a fairly constant fluorescence intensity. Superficially at least, this abrupt or episodic appearance of Golgi elements at peripheral sites in living cells is exactly analogous to the formation of VSV-G^{ts}–GFP–labeled vesicular–tubular structures at ER exit sites (Presley et al., 1997; Scales et al., 1997). This is positive evidence for the first test of our hypothesis.

Based on ultrastructural evidence, the newly formed Golgi elements during microtubule depolymerization must rapidly assume a stacked morphology; the frequency of stacked cisternal-like structures positive for GalNAc-T2 was at least as high, if not higher, than in untreated control cells. Neither the number of cisternae per stack nor the breath of individual stacked cisternae in cross section decreased. Peripheral Golgi stacks were polarized in their distribution of the *trans*-Golgi/TGN marker, GalT. What did change was that Golgi elements were no longer extensively interconnected. The peripheral Golgi stacks were frequently curved back on themselves in a structure we term onions. Such structures can be seen at a very low frequency in control cells and resemble intermediates in in vitro Golgi assembly (Rabouille et al., 1995*b*). The gradual accumulation of onion forms at peripheral sites during Golgi scattering is consistent with these structures being newly generated and suggests that a normal role of microtubules is to aid in the maintenance of a flattened, extended Golgi stack morphology. The slow and ultimately incomplete disappearance of spread, flattened Golgi stacks during microtubule depolymerization suggests that Golgi cisternae may well sequester or support the association of stabilizing molecules for long periods. Also, there may be some preferential association of residual, stable microtubules with spread individual Golgi stacks that may prevent the stack from curving back upon itself. Minin (1997) has suggested that drug-stable microtubules are important in Golgi scattering. Individual electron micrographs suggested an association between peripheral Golgi stacks and ER exit sites. In summary, these observations indicate a coalescence of Golgi proteins at peripheral sites within the cell to generate stacked Golgi cisternae. This is a process consistent with blocked juxtanuclear accumulation of cycling of Golgi transmembrane proteins.

To test whether nocodazole-scattered Golgi stacks exchange proteins with one another in a manner consistent with ER cycling, we took a photobleaching approach using both FRAP and FRAP-W protocols. FRAP experiments with GalNAc-T2–GFP and GalT–GFP indicated that Golgi-resident transmembrane proteins slowly cycle over tens of minutes between peripheral Golgi stacks. Since new protein synthesis was blocked by cycloheximide, the fluorescence recovery must be due to protein exchange between Golgi elements. Photorecovery had an apparent rate constant of $\sim 5 \times 10^{-12}$ cm^2/s, about three orders of magnitude slower than that expected for diffusion for

Golgi proteins within a continuous membrane system (Storrie et al., 1994; Cole et al., 1996*b*; Ellenberg et al., 1997; for reviews see Storrie and Kreis, 1996; Lippincott-Schwartz et al., 1998). In FRAP-W experiments in which GalNAc-T2–GFP or GalT–GFP fluorescence is photobleached over a large area of the cell and fluorescence loss over the nonbleached area is monitored as photorecovery occurs over the bleached area, essentially all peripheral Golgi stacks within the cell were shown to exchange proteins with one another. Here the total time period for protein equilibration between the scattered Golgi stacks was ~2 h. The peripheral Golgi structures did not collide with one another or form tubular interconnections. Imaging at high intensity illumination revealed movements through what appeared to be an ER network that were consistent with the ER being an intermediate in this ongoing Golgi protein exchange, a form of protein recycling. With respect to these photobleaching results, we would like to make clear that these assays provide no data on trafficking that occurs within a single Golgi stack, as such trafficking would be invisible in our assay because it does not produce protein exchange between physically separated Golgi units. In summary, these observations suggest a continuous cycling of Golgi transmembrane proteins between scattered Golgi stacks in microtubule-depolymerized cells. These experiments provide positive evidence for the second test of our hypothesis.

To provide direct experimental evidence for the ER being an intermediate in a slow Golgi protein cycling pathway, we tested the effects of expression of the plasmid pSar1p^{dn}CMUIV on the distribution of Golgi glycosyltransferases. This plasmid codes for a dominant-negative mutant of Sar1p, a protein required for ER export. Addition of Sar1p^{dn} has been previously shown to block ER export both in vitro (Aridor et al., 1995) and in vivo (Pepperkok et al., 1998; Shima et al., 1998). Shima et al. (1998) have previously shown that microinjection of His-tagged Sar1p^{dn} blocks ER export but that it has no major effects on the distribution of Golgi cisternal components in short-term experiments of ~1 h in duration. Based on the slow time scale of nocodazole-induced Golgi scattering, we deliberately assayed for Golgi effects on the slow time scale of multiple hours. Three key effects were noted in our experiments. First, preexisting Golgi structures, be they juxtanuclear or nocodazole scattered, as detected by immunofluorescent labeling for either GalNAc-T2–VSV or GalT disappeared over a time course of a few hours. Similar results have also been seen using transfected *N*-acetylglucosaminyltransferase I as a Golgi marker in Vero cells (Storrie, B., unpublished observations). Allowing for a 1–2-h Sar1p^{dn} expression period to produce sufficient protein to disrupt cell phenotype, we estimate a half-time of 2–3 h for the disappearance of the juxtanuclear Golgi staining. This half-time is reasonably consistent with the overall half-time of nocodazole-induced Golgi scattering and the kinetics of Golgi protein exchange in FRAP-W experiments. All these are processes encompassing most, if not all, of the scattered structures. Second, preexpression of Sar1p^{dn} inhibited the appearance of GalNAc-T2 in peripheral Golgi structures during nocodazole treatment. This is a result consistent with nocodazole-induced Golgi scattering through an ER recycling pathway. Third, disappearance of preexisting Golgi structures was accompanied by accumulation of GalNAc-T2–VSV in structures, giving an ER-like staining pattern. This ER distribution certainly included some newly synthesized GalNAc-T2. However, the bulk of the ER-trapped GalNAc-T2 was from preexisting proteins that recycled from the juxtanuclear Golgi apparatus or peripheral Golgi stacks. This contention is based on three lines of reasoning: (*a*) The GalNAc-T2 time kinetics for ER accumulation were too fast for more than a small fraction of the total ER GalNA-T2 to be newly synthesized; the majority must be pre-existing, metabolically stable, GalNAc-T2 redistributed to the ER. GalNAc-T2 antigenicity was shown to be metabolically stable in the presence of the potent protein synthesis inhibitors, cycloheximide and emetine. (*b*) Protein synthesis inhibitor–limited pulse expression of pSar1p^{dn} was sufficient to produce subsequent ER accumulation of juxtanuclear GalNAc-T2 in the continued presence of either cycloheximide or emetine. (*c*) Microinjection of the His-tagged Sar1p^{dn} in the presence of emetine followed by incubation in the continuous presence of emetine produced a similar ER accumulation. In summary, these observations strongly argue that Golgi cisternal proteins cycle to the ER with a half-time of a few hours. During nocodazole treatment, which causes microtubule depolymerization, this pathway continues at a substantial rate. These experiments provide positive evidence for the third and fourth tests of our hypothesis.

Our experiments indicate both a pronounced tendency for Golgi cisternal proteins to recycle normally to the ER and to assemble into polarized stacked Golgi cisternae. This is a conclusion entirely consistent with our fluorescence and electron microscopy studies. In particular, by electron microscopy the high labeling density of GalNAc-T2–VSV in transfected HeLa cells allowed us to relate structures to Golgi formation or cycling by content of GalNAc-T2. In these studies, we observed little significant increase in GalNAc-T2 labeling over the ER during the Golgi scattering process. These data are not surprising in view of the greater surface area of the ER relative to the Golgi and the apparent tendency of Golgi proteins to "self-associate" into peripheral Golgi stacks in nocodazole-treated cells. The membrane surface of the ER is about fivefold greater than that of the Golgi (Griffiths et al., 1984; Quinn et al., 1984). Any cycling Golgi protein entering the ER is diluted relative to its concentration in the Golgi complex. Depending on kinetics of various steps in an overall recycling process, the level of cycling Golgi protein found in the ER during Golgi scattering might not be significantly more than that in control non–drug-treated cells. From our fluorescence studies, Golgi proteins have a high tendency to clear from the ER into Golgi stacks. The ER step appears to be the rapid step within an otherwise slow overall pathway. In recent work, Cole et al. (1998) have shown recycling to the ER of a number of Golgi-localized VSV-G^{ts} chimeric proteins. Our present work is fully consistent with these observations. However, here we show ER recycling of Golgi glycosylation enzymes, which are resident type II transmembrane proteins, represent the major known class of Golgi transmembrane proteins and include all known Golgi glycosyltransferases and glycosidases. Hence, our demonstration has a particular rele-

vance to the functional and structural maintenance of the Golgi apparatus.

A Golgi-to-ER pathway presumably plays an important role in the normal recycling of resident Golgi membrane proteins that "leak" from the organelle. Protein retention and potential recycling within the Golgi complex are unlikely to be perfect. This pathway also has the potential to be a quality control device to select against damaged Golgi membrane proteins as they cycle through the ER. Also, the pathway may be a consequence of the necessity to recycle lipids back to the ER to be used in further rounds of transport and membrane assembly. The recycling of resident Golgi proteins to the ER might occur by direct transient fusions between Golgi and ER membranes. We could not detect vesicular carriers using a high-speed camera, though this cannot be formally ruled out. However, if recycling is through vesicular carriers, these would have to fuse directly with ER membranes. Regardless of the nature of the intermediates, it is clear that recycling Golgi components reside only briefly in the ER normally and can coalesce into a newly formed Golgi stack within minutes. As shown previously by immunofluorescence, this coalescence seems to be associated with structures that on the basis of their content of ERGIC53/p58 are likely to be located at or about ER exit sites (Cole et al., 1996*a*; Yang and Storrie, 1998; for review see Storrie and Yang, 1998). In conclusion, we have provided strong evidence for a novel Golgi-to-ER recycling pathway that gives a highly plausible explanation for the nature of Golgi scattering upon microtubule depolymerization. Establishing the mechanism and signals that regulate such a pathway will be a major challenge for the future.

This project was a joint effort between the laboratories of Brian Storrie at Virginia Tech and those of Ernst Stelzer and Tommy Nilsson at EMBL-Heidelberg. During this project, Jamie White and Sabine Röttger were predoctoral students at EMBL-Heidelberg, and the work of Jamie White was jointly sponsored by Ernst Stelzer and Tommy Nilsson and that of Sabine Röttger by Tommy Nilsson. At Virginia Tech-Blacksburg, we would like to express our appreciation to Jeffrey Bocock, Sarah Buss, Karen Capen, and Nolan Ko for quantification of various morphometric measurements and fluorescence intensities. At EMBL-Heidelberg, we would like to express our appreciation to the CCC developers: Nick Salmon, Alfons Riedinger, Georg Ritter, Stephan Albrecht, Thomas Stephany, and Reiner Stricker, to Ann Atzberger for FACS®, to Anja Habermann for cryosectioning, and to Joel Lanoix for his help on Sar1p^{dn} purification. We gratefully acknowledge the critical comments on the manuscript of Rich Walker and Brenda Shirley at Virginia Tech and of Joachim Füllekrug, Joel Lanoix, and Heidi McBride at EMBL-Heidelberg.

This work was supported in part by grants to the individual laboratories and by a grant to B. Storrie from the Fogarty International Center, U.S. National Institutes of Health while he was on sabbatical in Tommy Nilsson's laboratory.

Received for publication 27 March 1998 and in revised form 18 September 1998.

References

Aridor, M., S.J. Bannykh, T. Rowe, and W.E. Balch. 1995. Sequential coupling between COPII and COPI vesicle coats in endoplasmic reticulum to Golgi transport. *J. Cell Biol.* 131:875–893.

Axelrod, D., D.E. Koppel, J. Schlessinger, E. Elson, and W.W. Webb. 1976. Mobility measurement by analysis of fluorescence photobleaching recovery kinetics. *Biophys. J.* 16:1055–1069.

Burkhardt, J.K. 1998. The role of microtubule-based motor proteins in maintaining the structure and function of the Golgi complex. *Biochim. Biophys. Acta.* 1404:113–126.

Burkhardt, J.K., C.J. Echeverri, T. Nilsson, and R.B. Vallee. 1997. Overexpression of the dynamitin (p50) subunit of the dynactin complex disrupts dynein-dependent maintenance of membrane organelle distribution. *J. Cell Biol.* 139:469–484.

Cole, N.B., N. Sciaky, A. Marotta, J. Song, and J. Lippincott-Schwartz. 1996*a*. Golgi dispersal during microtubule disruption: regeneration of Golgi stacks at peripheral endoplasmic reticulum exit sites. *Mol. Biol. Cell.* 7:631–650.

Cole, N.B., C.L. Smith, N. Sciaky, M. Terasaki, M. Edidin, and J. Lippincott-Schwartz. 1996*b*. Diffusional mobility of Golgi proteins in membranes of living cells. *Science.* 273:797–801.

Cole, N.B., J. Ellenberg, J. Song, D. DiEuliis, and J. Lippincott-Schwartz. 1998. Retrograde transport of Golgi localized proteins to the ER. *J. Cell Biol.* 140: 1–15.

Doms, R.W., G. Russ, and J.W. Yewdell. 1989. Brefeldin A redistributes resident and itinerant Golgi proteins to the endoplasmic reticulum. *J. Cell Biol.* 109:61–72.

Dunphy, W.G., and J.E. Rothman. 1983. Compartmentation of asparagine-linked oligosaccharide processing in the Golgi apparatus. *J. Cell Biol.* 97: 270–275.

Dunphy, W.G., E. Fries, L.J. Urbani, and J.E. Rothman 1981. Early and late functions associated with the Golgi apparatus reside in distinct compartments. *Proc. Natl. Acad. Sci. USA.* 78:7453–7457.

Ellenberg, J., E.J. Siggia, J.E. Moreira, C.L. Smith, J.F. Presley, H.J. Worman, and J. Lippincott-Schwartz. 1997. Nuclear membrane dynamics and reassembly in living cells: targeting of an inner nuclear membrane protein in interphase and mitosis. *J. Cell Biol.* 138:1193–1206.

Füllekrug, J., and T. Nilsson. 1998. Protein sorting in the Golgi complex. *Biochim. Biophys. Acta.* 1404:77–84.

Griffiths, G., G. Warren, P. Quinn, O. Mathieu-Costello, and H. Hoppeler. 1984. Density of newly synthesized plasma membrane proteins in intracellular membranes. I. Stereological studies. *J. Cell Biol.* 98:2133–2141.

Ho, W.C., V.J. Allan, G. Van Meer, E.G. Berger, and T.E. Kreis. 1989. Reclustering of scattered Golgi elements occurs along microtubules. *Eur. J. Cell Biol.* 48:250–263.

Ho, W.C., B. Storrie, R. Pepperkok, W. Ansorge, P. Karecla, and T.E. Kreis. 1990. Movement of interphase Golgi apparatus in fused mammalian cells and its relationship to cytoskeletal elements and rearrangement of nuclei. *Eur. J. Cell Biol.* 52:315–327.

Kreis, T.E. 1986. Microinjected antibodies against the cytoplasmic domain of vesicular stomatitis virus glycoprotein block its transport to the cell surface. *EMBO (Eur. Mol. Biol. Organ.) J.* 5:931–941.

Lippincott-Schwartz, J., L.C. Yuan, J.S. Bonifacino, and R.D. Klausner. 1989. Rapid redistribution of Golgi proteins into the ER in cells treated with brefeldin A: evidence for membrane cycling from Golgi to ER. *Cell.* 56:801–813.

Minin, A.A. 1997. Dispersal of Golgi apparatus in nocodazole-treated fibroblasts is a kinesin-driven process. *J. Cell Sci.* 110:2495–2505.

Nichols, B.J., and H.R.B. Pelham. 1998. SNAREs and membrane fusion in the Golgi apparatus. *Biochim. Biophys. Acta.* 1404:9–31.

Nilsson, T., M. Jackson, and P.A. Peterson. 1989. Short cytoplasmic sequences serve as retention signals for transmembrane proteins in the endoplasmic reticulum. *Cell.* 58:707–718.

Nilsson, T., M. Pypaet, M.H. Hoe, P. Slusarewicz, E.G. Berger, and G. Warren. 1993. Overlapping distribution of two glycosyltransferases in the Golgi apparatus of HeLa cells. *J. Cell Biol.* 120:5–13.

Pääbo, S., F. Weber, T. Nilsson, W. Schaffner, and P.A. Peterson. 1986. Structural and functional dissection of an MHC class I antigen-binding adenovirus glycoprotein. *EMBO (Eur. Mol. Biol. Organ.) J.* 5:1921–1927.

Palade, G. 1975. Intracellular aspects of the process of protein secretion. *Science.* 189:347–358.

Parton, R.G., K. Simon, and C.G. Dotti. 1992. Axonal and dendritic endocytic pathways in cultured neurons. *J. Cell Biol.* 119:123–137.

Pepperkok, R., M. Lowe, B. Burke, and T.E. Kreis. 1998. Three distinct steps in transport of vesicular stomatitis virus glycoprotein from the ER to the cell surface in vivo with differential sensitivities to GTPγS. *J. Cell Sci.* 111:1877–1888.

Perlman, S., and S. Penman. 1970. Mitochondrial protein synthesis: resistance to emetine and response to RNA synthesis inhibitors. *Biochem. Biophys. Res. Commun.* 40:941–948.

Presley, J.F., N.B. Cole, T.A. Schroer, K. Hirschberg, K.J.M. Zaal, and J. Lippincott-Schwartz. 1997. ER-to-Golgi transport visualized in living cells. *Nature.* 389:81–85.

Quinn, P., G. Griffiths, and G. Warren. 1984. Density of newly synthesized plasma membrane proteins in intracellular membranes II. Biochemical studies. *J. Cell Biol.* 98:2142–2147.

Rabouille, C., N. Hui, F. Hunte, R. Kieckbusch, E.G. Berger, G. Warren, and T. Nilsson. 1995*a*. Mapping the distribution of Golgi enzymes involved in the construction of complex oligosaccharides. *J. Cell Sci.* 108:1617–1627.

Rabouille, C., T. Mistelli, R. Watson, and G. Warren. 1995*b*. Reassembly of Golgi stacks from mitotic Golgi fragments in a cell-free system. *J. Cell Biol.* 129:605–618.

Rambourg, A., and Y. Clermont. 1990. Three-dimensional electron microscopy: structure of the Golgi apparatus. *Eur. J. Cell Biol.* 51:189–200.

Roth, J., and E.G. Berger. 1982. Immunocytochemical localization of galactosyltransferase in HeLa cells: codistribution with thiamine pyrophosphates in the *trans*-Golgi cisternae. *J. Cell Biol.* 93:223–229.

Rothman, J.E. 1994. Mechanisms of intracellular protein transport. *Nature.* 372: 55–63.

Röttger, S., J. White, H.H. Wandall, J.-C. Olivo, A. Stark, E.P. Bennett, C. Whitehouse, E.G. Berger, H. Clausen, and T. Nilsson. 1998. Localization of three human polypeptide GalNAc-transferases in HeLa cells suggests initiation of O-linked glycosylation throughout the Golgi apparatus. *J. Cell Sci.* 111:45–60.

Rowe, T., and W.E. Balch. 1995. Expression and purification of mammalian Sar1. *Methods Enzymol.* 257:49–53.

Scales, S.J., R. Pepperkok, and T.E. Kreis. 1997. Visualization of ER-to-Golgi transport in living reveals a sequential mode of action for COPII and COPI. *Cell.* 90:1137–1148.

Sciaky, N., J. Presley, C. Smith, K.J.M. Zaal, N. Cole, J.E. Moreira, M. Terasaki, E. Siggia, and J. Lippincott-Schwartz. 1997. Golgi tubule traffic and the effects of brefeldin A visualized in living cells. *J. Cell Biol.* 139:1–18.

Shima, D.T., K. Haldar, R. Pepperkok, R. Watson, and G. Warren. 1997. Partitioning of the Golgi apparatus during mitosis in living HeLa cells. *J. Cell Biol.* 137:1211–1228.

Shima, D.T., N. Cabrera-Poch, R. Pepperkok, and G. Warren. 1998. An ordered inheritance strategy for the Golgi apparatus: visualization of mitotic disassembly reveals a role for the mitotic spindle. *J. Cell Biol.* 141:955–966.

Storrie, B., and T.E. Kreis. 1996. Probing the mobility of membrane proteins inside the cell. *Trends Cell Biol.* 6:321–324.

Storrie, B., and W. Yang. 1998. Dynamics of the interphase mammalian Golgi complex as revealed through drugs producing reversible Golgi disassembly. *Biochim. Biophys. Acta.* 1404:127–138.

Storrie, B., R. Pepperkok, E.H.K. Stelzer, and T.E. Kreis. 1994. The intracellular mobility of a viral membrane glycoprotein measured by confocal microscope fluorescence recovery after photobleaching. *J. Cell Sci.* 107:1309–1319.

Tokuyasu, K.T. 1998. A study of positive staining of ultrathin frozen sections. *J. Ultrastruct. Res.* 63:287–307.

Turner, J.R., and A.M. Tartakoff. 1989. The response of the Golgi complex to microtubule alterations: the roles of metabolic energy and membrane traffic in Golgi complex organization. *J. Cell Biol.* 109:2081–2088.

Watzele, G., R. Bachoner, and E.G. Berger. 1991. Immunocytochemical localization of the Golgi apparatus using protein-specific antibodies to galactosyltransferase. *Eur. J. Cell Biol.* 56:451–458.

Weibel, E.R. 1979. Stereological Methods. I. Practical Methods for Morphometry. Academic Press, London. 415 pp.

Yang, W., and B. Storrie. 1998. Scattered Golgi elements during microtubule disruption are initially enriched in trans Golgi proteins. *Mol. Biol. Cell.* 9:191–207.